September 1, 1992

Technical Report
Project RF 4502

Compressible and Incompressible Fluid Seals: Influence on Rotordynamic Response and Stability

The flow field inside a whirling annular seal operating a Reynolds numbers of 12,000 and 24,000 and a Taylor number of 6,600 has been measured. The rotor was mounted eccentric (50%) upon the test facilities shaft which resulted in a circular orbit at a whirl ratio of 1.0. Mr. Howard D. Thames III completed these measurements and wrote his Master of Science thesis during the present year. Using the information in his thesis, three papers which summarize the work were written and presented at three different conferences. The three papers are attached.

Addition measurements have been performed for the annular seal operating at an eccentricity ratio of 10% for Re=24,000 and Ta=6,600. A labyrinth seal was also installed into the facility and operated at an eccentricity ratio of 50% at the same Reynolds and Taylor numbers. These data are currently being reduced and analyzed.

Experimental Study of the Flow Field Inside a Whirling Annular Seal

by

Gerald L. Morrison, Professor
Robert E. DeOtte, Jr., Research Engineer
H. Davis Thames III, Graduate Student

Presented At:

4th International Symposium on
Transport Phenomena and
Dynamics in Rotating Machinery

April 5-8, 1992
Honolulu, Hawaii

Experimental Study of the Flow Field Inside a Whirling Annular Seal

Gerald L. Morrison, Professor
Robert E. DeOtte, Jr., Research Engineer
H. Davis Thames III, Graduate Student
Turbomachinery Laboratory
Mechanical Engineering Department
Texas A&M University
College Station, Texas 77843-3123

ABSTRACT

The flow field inside a whirling annular seal has been measured using a 3-D Laser Doppler Anemometer (LDA) system. The seal investigated has a clearance of 1.27 mm, a length of 37.3 mm and is mounted on a drive shaft with a 50% eccentricity ratio. This results in the rotor whirling at the same speed as the shaft rotation (whirl ratio = 1.0). The seal is operated at a Reynolds number of 12,000 and a Taylor number of 6,300 (3,600 rpm). The 3-D LDA system is equipped with a rotary encoding system which is used to produce phase averaged measurements of the entire mean velocity vector field and Reynolds stress tensor field from 0.13 mm upstream to 0.13 mm downstream of the seal. The mean velocity field reveals a highly three dimensional flow field with large radial velocities near the inlet of the seal as well as a recirculation zone on the rotor surface. The location of maximum mean axial velocity migrates from the pressure side of the rotor at the inlet to the suction side at the exit. Turbulence production is a maximum near the seal inlet as indicated by the rapid increase of the turbulence kinetic energy (κ). However, turbulence production and dissipation attain equilibrium fairly quickly with κ remaining relatively constant over the last half of the seal.

NOMENCLATURE

A = leakage area, πDc, m^2
c = nominal clearance between the rotor and stator = R2-R1, m
D = stator diameter, m
L = rotor length, m
Q = leakage rate, m^3/s
Re = Reynolds number = $2\rho Uc/\mu$
R1 = rotor radius, m
R2 = stator radius = D/2, m
Ta = Taylor number = $[\rho W_{sh} c/\mu][2c/D]^{\frac{1}{2}}$
U = average leakage velocity = Q/A, 3.71 m/s
U_x = axial mean velocity, m/s
U_r = radial mean velocity, m/s
U_θ = azimuthal mean velocity, m/s

$\overline{u_x' u_x'}$ = axial time averaged Reynolds normal stress, m^2/s^2

$\overline{u_r' u_r'}$ = radial time averaged Reynolds normal stress, m^2/s^2

$\overline{u_\theta' u_\theta'}$ = azimuthal time averaged Reynolds normal stress, m^2/s^2

W_{sh} = azimuthal velocity of the rotor surface, 30.9 m/s

X = axial distance from seal inlet, m

θ = azimuthal angle measured from the minimum clearance in the direction of shaft rotation, clockwise on the figures

κ = turbulence kinetic energy = $\frac{1}{2}(\overline{u_x' u_x'}+\overline{u_r' u_r'}+\overline{u_\theta' u_\theta'})$, m^2/s^2

μ = absolute viscosity of the fluid (water), Ns/m^2

ρ = fluid density, Kg/m^2

( )' = fluctuating value = instantaneous value - mean value

$\overline{(\ )}$ = mean value (time averaged)

INTRODUCTION

The influence of seals upon the rotordynamic stability of turbomachines has become an important concern in the last 20 years as turbomachines have become lighter and have been required to operate at increasingly higher speeds. This was clearly demonstrated on the Space Shuttle Main Engines (SSME) where the seals became a critical element in the stable operation of the turbomachine. Accurately predicting the leakage rate through a seal is an extremely difficult task due to the great number of geometric variables as well as harsh operating conditions and exotic fluids. Such complexity pushed the limits of empirical and bulk flow models. Now with the additional requirement of knowing the forces generated by the seal and how they effect the rotordynamic stability, a new generation of analyses is needed.

To address this challenge, Tam, Przekwas, Muszynska, Hendricks, Braun, and Mullen[1] undertook a numerical and analytical study of the fluid dynamic forces in seals and bearings. They solved the Reynolds averaged Navier-Stokes equations for the turbulent, swirling flow field inside annular seals using the PHOENICS-84 numerical code. In their study[1], the effects of preswirl, whirl ratio, overall pressure drop, shaft speed, fluid injection, and eccentricity ratio upon the flow field were examined and an evaluation of the resultant fluid dynamic forces generated by the seal was performed. These calculated forces and overall leakage rates were then compared with measurements performed by Childs[2,3]. Overall, good agreement was obtained.

OBJECTIVES

There is one obstacle standing in the way of further advancement of this type of computational analysis - the turbulence model. The statement of Tam, et.al.[1], "until fluctuation details for high shear flows at low clearances become available the simplest of the turbulence models was selected for the present calculations," indicates a need for more detailed basic information. In order to adequately evaluate the effectiveness of the turbulence model, details of the flow field (velocity field and the Reynolds stress tensor) are required. It is the objective of an ongoing research project at the Turbomachinery Laboratory, funded by NASA Lewis, to obtain this required data. Presented in this paper is a portion of the results. In particular, the distributions for the three mean velocity components and the turbulence kinetic energy level are presented for one axial location immediately upstream of the seal inlet and five axial positions along the length of the seal. Additional information, including the Reynolds stress tensor, was obtained at various other axial locations; space limitations, however, prohibit the presentation of all this information in one paper. The data are available on MS-DOS disks and a more complete presentation is available in Mr. H.D. Thames' thesis[4].

FACILITIES AND INSTRUMENTATION

The facility used in this investigation has been previously described in detail by Morrison[5,6]. Briefly, the test section (Figure 1) consists 50.4 mm diameter overhung shaft directly coupled to a 37 kW electric

induction motor. The electric motor is driven by a power supply capable of varying speeds from 200 to 5,300 rpm. The seal itself is composed of an acrylic rotor (0.164 m O.D.) and a stainless steel stator with a nominal clearance between the rotor and stator that is 1.27 mm. The rotor is optically coated by a vacuum-deposition technique to reduce reflected light intensity and is mounted on the stainless steel shaft using a brass bushing, the outer circumference of which is 0.63 mm eccentric with reference to the axis of the shaft. This results in the rotor being eccentric causing whirl in a circular orbit at the same speed as the shaft (whirl ratio 1.0). The seal stator is constructed of stainless steel with a smooth finish. To permit access for the LDA system, a flat optical window is installed in a narrow slit along the axis of the seal. A flat window is used to avoid lens effects. The deviation from roundness resulting from the window is only 1.5% of the clearance or 0.027% of the rotor radius. The annular seal is a constant radius design which is 37.3 mm long.

A 3.75 m^3 storage tank supplies water at approximately 300 K to a centrifugal pump. The pump flow rate of 0.00243 m^3/s is set by a throttling valve and metered by a turbine flow meter. After metering, the water is introduced into the seal rig and water exiting the seal is returned to the storage tank. Expansel 462 WU, 6 μm diameter plastic sphere with a specific gravity of 1.23, is added to the water to provide light scattering seed for the laser Doppler anemometer system. This particle will follow instantaneous flow fluctuations up to 44,000 Hz.

Morrison, et al [5,6] have previously discussed in detail the 3-D LDA system used and have presented an error analysis for the system. The LDA system is a three color, six beam arrangement with 8.5X beam expanders. Two colors measure orthogonal velocity components and the optical axis for the third color is inclined at 30° to the others. This results in a measurement volume 0.025 X 0.025 X 0.10 mm in size. Bragg cells are installed on one beam of each color pair so that flow reversals can be measured. This LDA system is thus capable of measuring the instantaneous 3-D velocity vector at the measurement volume. The data acquisition systems consists of a rotating machinery resolver and three counters which supply the angle of the rotor as well as the three non-orthogonal velocity components to an 80386 computer system. A gate on the master interface assures that all three counters measure a velocity component within a coincidence window of 10 μs. The data is then post processed to calculate the mean velocity, Reynolds stress tensor, and other quantities with the data divided into 20 different angular positions of the rotor, each with a window of 18° (one window had inadequate data for analysis). A minimum of 90,000 velocity realizations sorted into the different angular positions of the rotor were recorded at each X and r location. This resulted in a minimum of 1000 and a maximum of approximately 8000 samples at each reported location for a given phase window. Figure 2 presents the locations on the r-θ plane where the measurements were made.

Recent experience (Wiedner[7] and Morrison[8]) with this system has shown that there is some velocity bias present in the data which is best corrected using the McLaughlin-Tiederman[9] velocity bias correction technique. Uncertainties are estimated[5] to be $\pm 1\%$ on $\bar{U}_x$ and $\bar{U}_\theta$, $\pm 2\%$ on $\bar{U}_r$, and 20% on κ.

RESULTS

Isovels were calculated from the data for the axial ($\bar{U}_x$), radial ($\bar{U}_r$), and azimuthal ($\bar{U}_\theta$) mean velocity components at X/L = -0.0018, 0.00, 0.21, 0.50, 0.77, and 1.00. Plots of these are presented in Figures 3-5. The rotor is orbiting in the clockwise direction (increasing θ).

The seal influences the mean velocity field immediately upstream (X/L = -0.018) of the inlet in two ways. First, because the large end of the rotor is exposed to the supply plenum, there is an induced preswirl which varies from 6% of the rotor surface speed ($0.06W_{sh}$, 0.50U) near the stator wall to 28% near the rotor. Secondly, the flow accelerates into the seal with the maximum axial velocity (1.3U) occurring near θ = 105° rather than at the maximum clearance location (θ = 180°). With the rotor spinning clockwise, it appears that fluid approaching the inlet at the region of maximum clearance maintains the axial momentum necessary to enter the seal but must accelerate as it is rotated into the smaller gap. This hypothesis is further substantiated in the analysis of the axial velocity contours at X/L = 0.00 where the fluid is semi-confined yet the precession of the rotor causes the axial velocity to increase even more (2.4U) as the clearance decreases ($\theta \approx 75°$). It is interesting that the fluid not only continues flowing downstream as the clearance decreases but actually experiences this substantial increase in local axial velocity. This is consistent with continuity since the azimuthal velocity remains small compared to the axial velocity at this azimuthal location. In this region, large outward radial velocities (0.9U) are caused by the rotor

moving toward the stator. In fact, the $\bar{U}_r$-$\bar{U}_\theta$ velocity vector in this plane is almost entirely in the outward radial direction for the rotor phase $30° \leq \theta \leq 180°$. This combined with the steep $\partial\bar{U}_x/\partial r$ near the rotor indicate the presence or onset of a flow separation on the rotor (as evidenced by the close spacing of the contours).

On the opposite side of the rotor (the phase where the clearance is increasing, $\theta > 180°$), the mean axial velocity decreases as θ increases until there is a negative axial velocity component (flow from the seal back into the plenum) from $\theta = 270°$ to 350°. The minimum velocity is -0.4U at X/L = -0.018 and -0.3U at X/L = 0.00. This side of the rotor ($180° < \theta < 360°$) is typically called the suction side. Therefore, one might expect this region where the clearance is increasing to provide less resistance to flow and to "suck in" fluid which would result in a positive $\bar{U}_x$. However, in this case, a strong azimuthal velocity component, $\bar{U}_\theta$, is bringing fluid into the widening clearance at a faster rate than the expansion can support causing a pressure increase. This results in the fluid actually "squirting out" of the seal back into the inlet plenum.

Progressing from X/L = 0.00 to 0.21, the region of maximum $\bar{U}_x$ moves counter-clockwise to $\theta \approx 90°$ and outward radially while decreasing in maximum value from 2.4U to 1.5U. The region occupied by the high speed flow is more uniform with smaller $\partial\bar{U}_x/\partial r$ gradients near the rotor indicating the reattachment of the flow to the rotor. $\bar{U}_x$ is positive across the entire cross-section with a minimum value of 0.2U, which indicates that a stagnation zone exists somewhere between X/L = 0.00 and 0.21. The radial velocities have become less than 10% of U compared to 80% at X/L = 0.00 indicating the flow is becoming more parallel to the stator. The azimuthal velocity distribution is much more uniform around the rotor being almost symmetric about $\theta = 0°$.

By the center of the seal, X/L = 0.50, $\bar{U}_x$ has been redistributed with the decreasing maximum velocity shifting clockwise. The flow is becoming established with the mean axial velocity being very nearly uniform over the entire seal and the radial velocity decreasing even further in amplitude to 0.04U. The azimuthal velocity distribution remains very much the same as at X/L = 0.21 except that there is a slight overall increase in magnitude.

The axial velocity component, $\bar{U}_x$, continues to show development by actually rotating locations of maximum value (1.5U) to $\theta \approx 315°$, where the backflow existed in the inlet, and the minimum $\bar{U}_x$ (0.4U) occurring where the maximum was present at the inlet. The radial velocities have increased slightly with a longer cross section of the flow having +0.04U. In the transition from X/L = 0.21 to 0.77 the regions of positive and negative radial velocity have exchanged places. The azimuthal velocity has increased slightly since X/L = 0.50 attaining approximately 35% of the shaft speed for $\theta < 90°$ and 25% for $\theta > 200°$. The azimuthal velocity distribution is the driving mechanism for the change in location of maximum mean axial velocity. From X/L = 0.50 to the end of the seal, $\bar{U}_\theta$ is consistently larger for $\theta < 180°$. This causes a migration of the fluid with the maximum $\bar{U}_x$ from $\theta \approx 75°$ at the inlet to $\theta \approx 315°$ at X/L = 0.77. This effect continues until the exit of the seal where $\bar{U}_x$ attains the maximum value of 1.9U and the minimum value of 0.3U. In the exit plane the radial velocities begin to rise in value as the flow begins to rearrange for the step change in area at the exit.

One of the variables calculated in most turbulence models is the turbulence kinetic energy ($\kappa = \frac{1}{2}\{\overline{u_x u_x} + \overline{u_r u_r} + \overline{u_\theta u_\theta}\}$). It is a good measure of the level of turbulence present in the seal. As mentioned earlier, we have measured the entire Reynolds stress tensor which is available in Thames[4]. The contours of κ presented in Figure 6 show that immediately upstream of the seal, the turbulence level is large with a maximum $\kappa = 0.4U^2$. This corresponds to a turbulence intensity which is approximately 50% of the average leakage velocity (U). This occurs near the rotor at $\theta = 270°$ where $\bar{U}_x$ is zero. Over the majority of the field, κ ranges from $0.2U^2$ to $0.3U^2$ (35% to 45% turbulence intensity), however, once the flow enters the seal, the turbulence kinetic energy increases rapidly in the region near the rotor where the mean flow appears to separate, and hence κ exceeds $0.8U^2$. This is consistent with the very large radial gradient of the mean axial velocity ($\partial\bar{U}_x/\partial r$) which contributes to the production of turbulence. As the flow progresses further downstream the turbulence kinetic energy levels decrease to approximately $0.3U^2$ at X/L = 0.21 and $0.2U^2$ for $0.50 \leq X/L \leq 1.00$. This relatively gradual change is expected since the spatial gradients of the mean velocity are significantly smaller for $x/L \geq 0.21$ hence the mechanism for turbulence production is reduced and turbulence dissipation begins to balance the turbulence production.

CONCLUSIONS

The flow field inside a whirling annular seal has been measured using a 3-D LDA system. The mean velocity field reveals a highly three dimensional flow field with large radial velocities near the inlet of the seal and a recirculation zone on the rotor surface. Near the inlet the mean axial velocity is very large on the pressure side of the rotor but by the downstream half of the seal, the region of high mean axial velocity has migrated to the suction side. Near the inlet, on the suction side of the rotor, there is a back flow into the plenum which is caused by the large azimuthal velocity moving large quantities of fluid into the region which then "spill over" into the plenum. The radial velocities steadily decrease in value as the flow progresses through the seal until the exit plane is reached at which point they increase abruptly, however, the magnitude is still significantly lower than at the inlet. The overall azimuthal velocity steadily increases from approximately $0.12W_{sh}$ at the inlet to $0.30W_{sh}$ at the exit. The flow over the seal inlet produces very large levels of turbulence kinetic energy. However, turbulence production and dissipation attain equilibrium fairly quickly and κ remains relative constant over the last half of the seal.

ACKNOWLEDGMENT

This work is supported by the NASA Lewis Research Center (NAG3-181) under the supervision of Mr. Robert C. Hendricks.

REFERENCES

1 Tam, L.T., Przekwas, A.J., Muszynska, A., Hendricks, R.C., Braun, M.J., and Mullen, R.L., "Numerical and Analytical Study of Fluid Dynamic Forces in Seals and Bearings," *Transaction of the ASME - Journal of Vibration, Acoustics, Stress, and Reliability in Design*, Vol. 110, July 1988, pp. 315-325.

2 Childs, D.W., Vance, J.M., and Hendricks, R.C., eds, *Rotordynamic Instability Problems in High Performance Turbomachinery*, Proceedings of the Workshop held at Texas A&M University; NASA CP-2238, 1982.

3 Childs, D.W., "SSME HPFTP Interstage Seals: Analysis and Experiments for Leakage and Reaction Force Coefficients," NASA Contract NASB-33716. Turbomachinery Laboratories, Texas A&M University, February, 1983.

4 Thames, H.D., "Mean Flow and Turbulence Characteristics in Whirling Annular Seals", Master of Science Thesis, Texas A&M University, Mechanical Engineering Department, May 1992.

5 Morrison, G.L., Johnson, M.C., and Tatterson, G.B., "Three-Dimensional Laser Anemometer Measurements in an Annular Seal," *Transactions of the ASME - Journal of Tribology*, Vol 113, July 1991, pp. 421-427.

6 Morrison, G.L., Johnson, M.C., and Tatterson, G.B., "3-D Laser Anemometer Measurements in a Labyrinth Seal," *Transactions of the ASME - Journal of Engineering for Gas Turbines and Power*, Vol 113, January 1991, pp. 119-125.

7 Wiedner, B.G., "Experimental Investigation of Velocity Biasing in Laser Doppler Anemometry," Master of Science Thesis, Texas A&M University, Mechanical Engineering Department, December, 1988.

8 Morrison, G.L., DeOtte, R.E., Jr., Nail, G.H., and Panak, D.L., "Mean Velocity Field and Turbulence Characterization of the Flow in an Orifice Flow Meter," *Laser Anemometry, Advances and Applications*, Vol. 1, August 1991, pp. 1-10.

9 McLaughlin, D.K., and Tiederman, W.G., "Biasing Correction for Individual Realization of Laser Anemometer Measurements in Turbulent Flows," *Physics of Fluids*, Vol. 16, 1973, p. 2082.

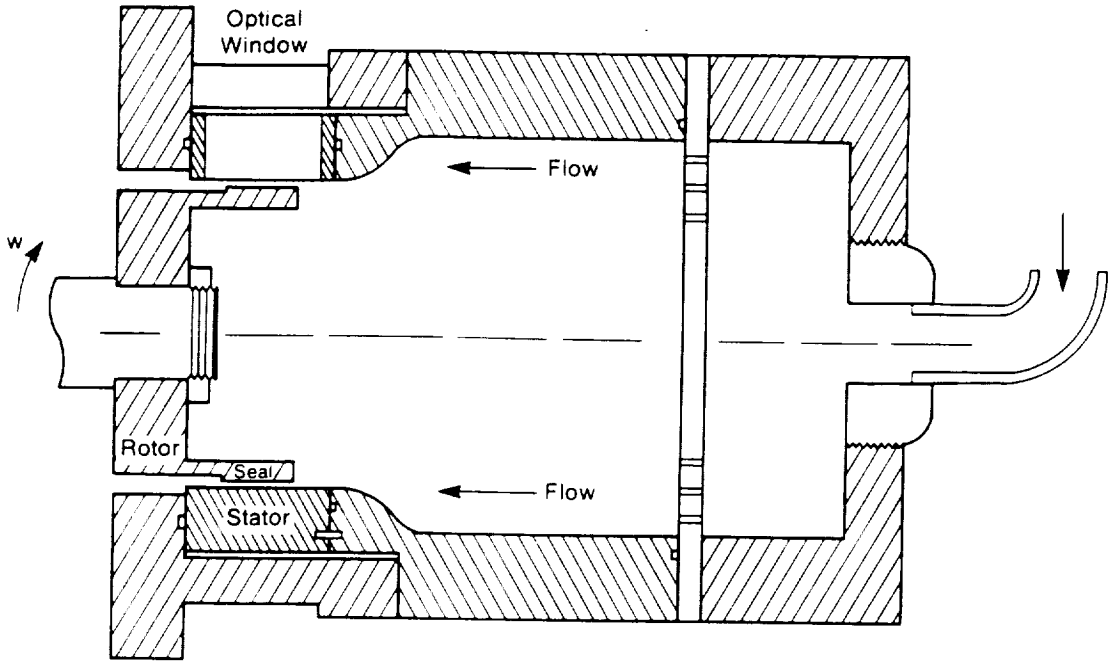

Figure 1 Test Section

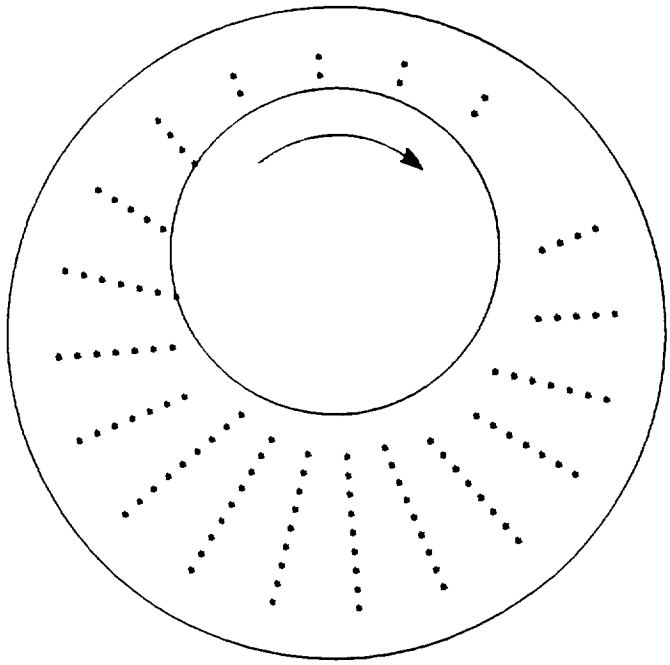

Figure 2 Measurement Grid

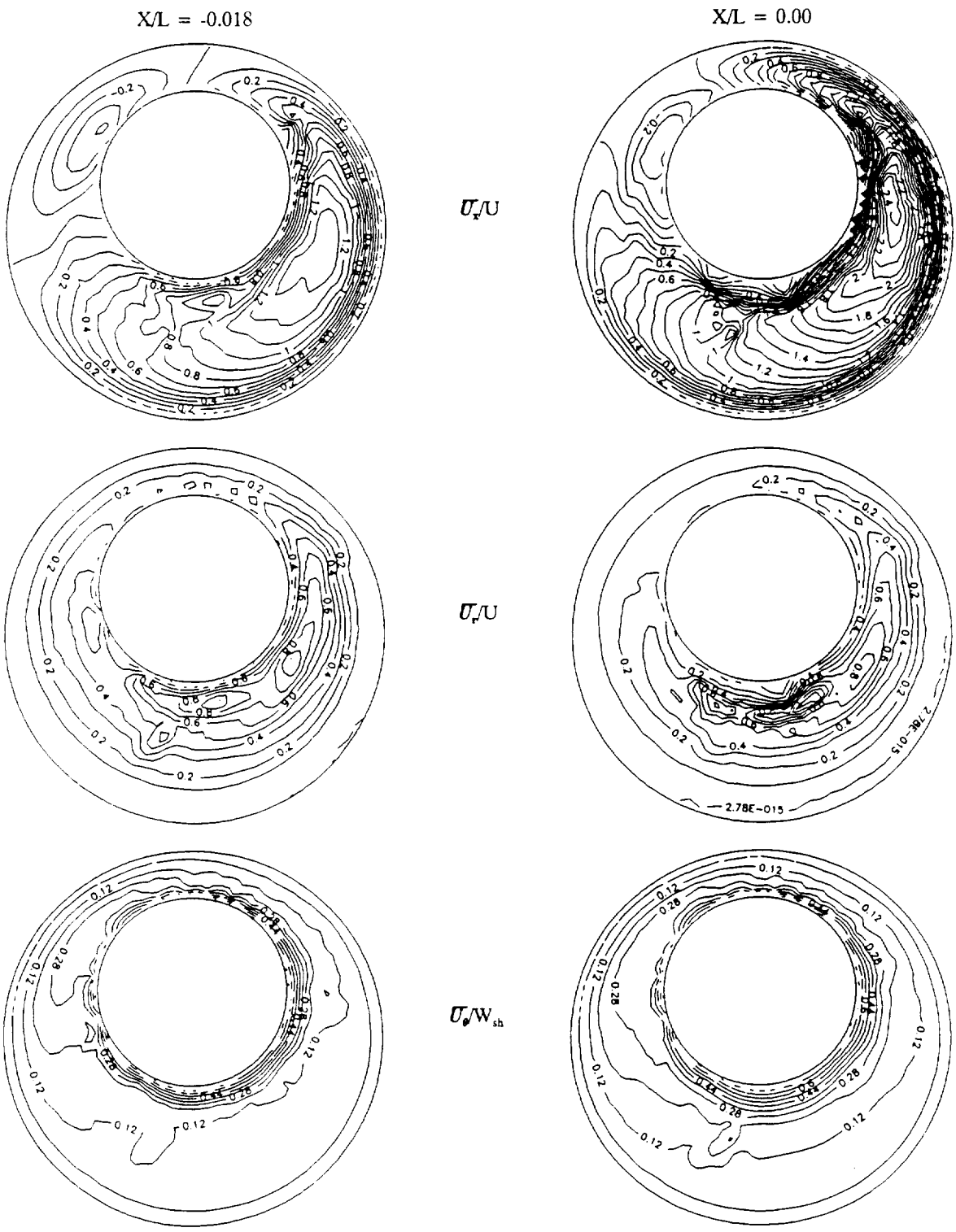

Figure 3 Mean Velocity Isovels, X/L = -0.018 and 0.00

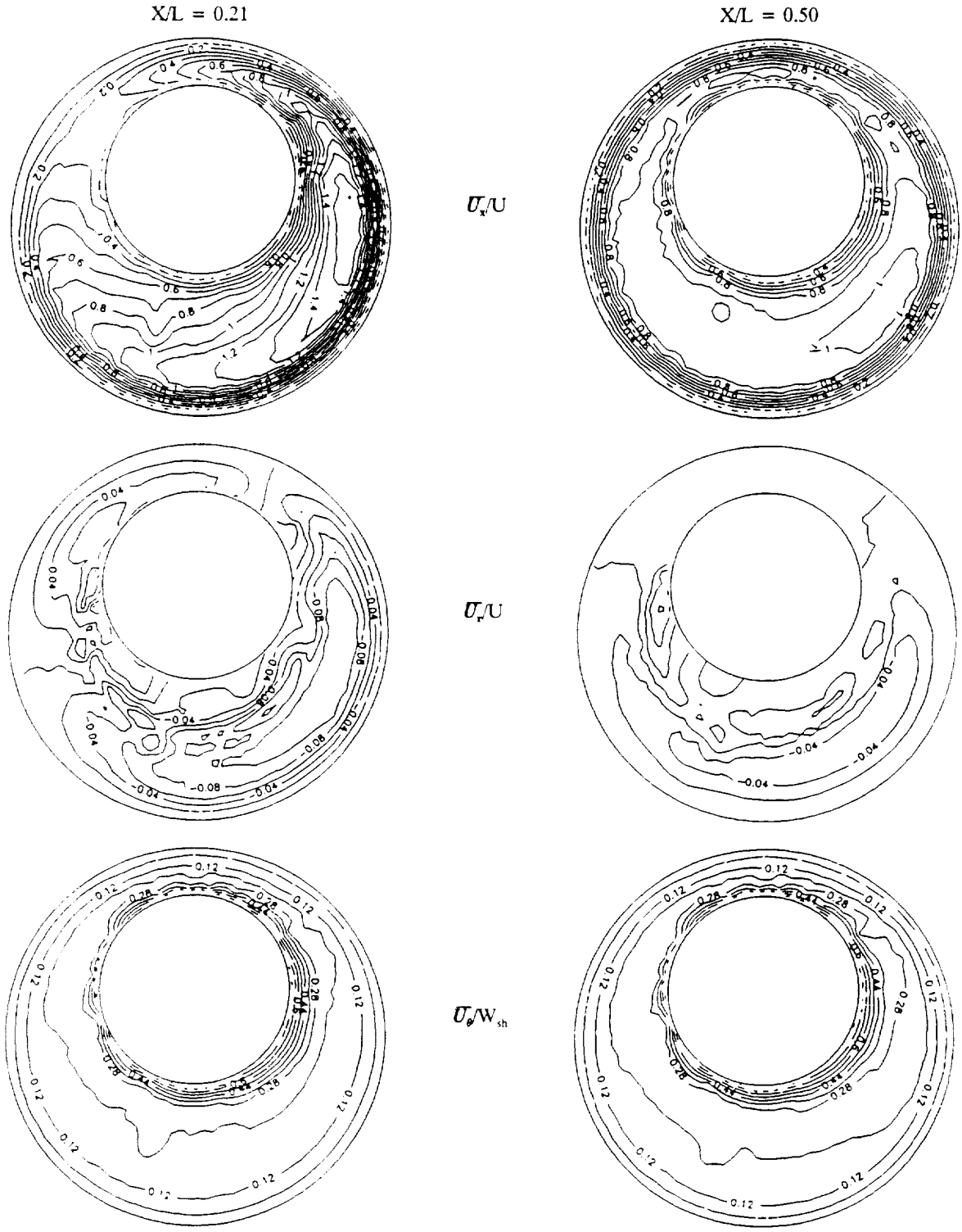

Figure 4 Mean Velocity Isovels, X/L = 0.21 and 0.50

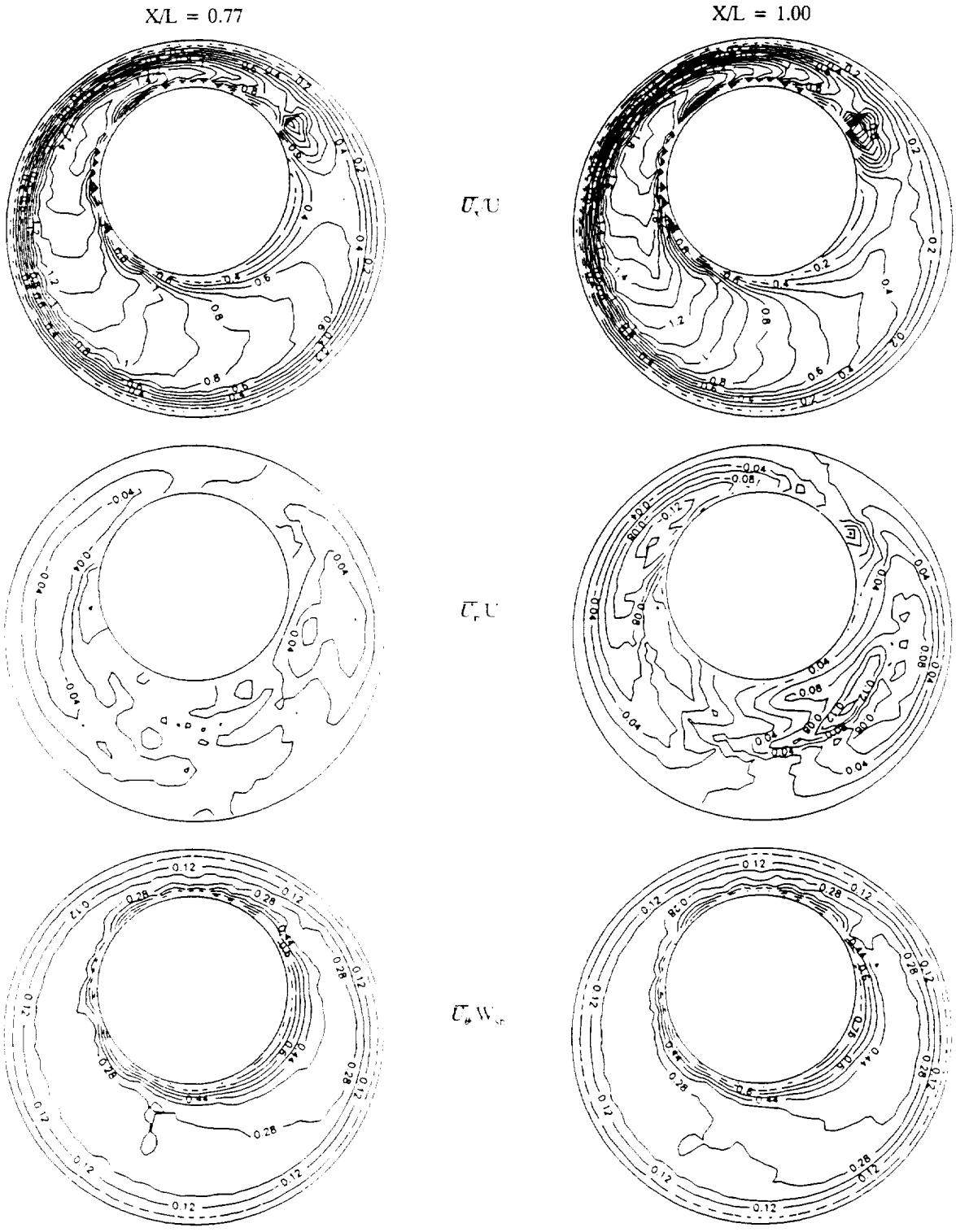

Figure 5 Mean Velocity Isovels, X/L = 0.77 and 1.00

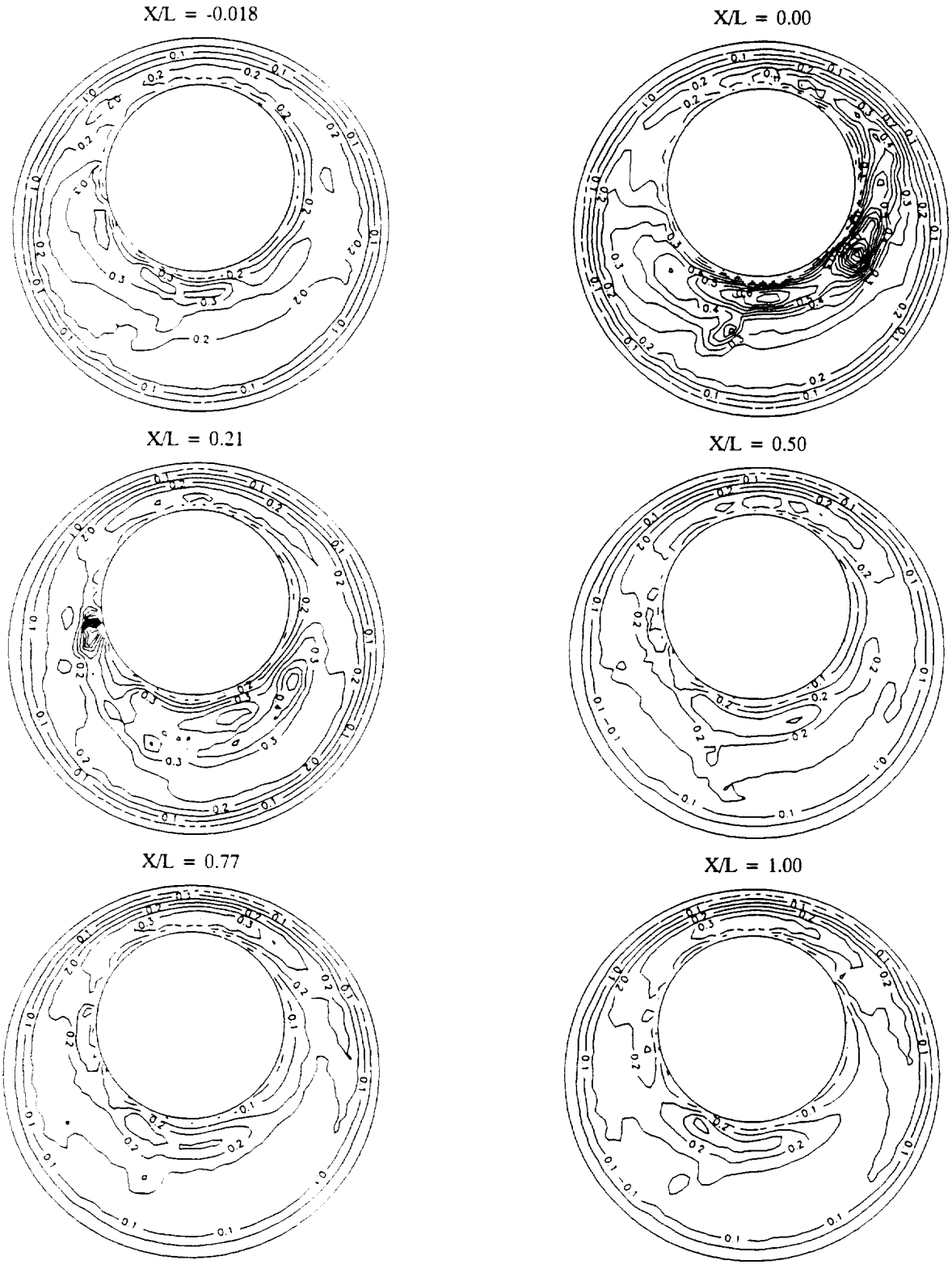

Figure 6 Turbulence Kinetic Energy, κ/U^2

Turbulence Measurements of High Shear Flow Fields in a Turbomachine Seal Configuration

by

Gerald L. Morrison, Professor
Robert E. DeOtte, Jr., Research Engineer
H. Davis Thames III, Graduate Student
Mechanical Engineering Department
Turbomachinery Laboratory
Texas A&M University
College Station, Texas 77843

Presented at

1992 Conference on
Advanced Earth-To-Orbit
Propulsion Technology

May 19-21, 1992
Huntsville, Alabama

Turbulence Measurements of High Shear Flow Fields in a Turbomachine Seal Configuration

G.L. Morrison, R.E. DeOtte, Jr., and H.D. Thames, III[1]
Texas A&M University
Mechanical Engineering Department
College Station, Texas 77845-3123

ABSTRACT

The mean velocity and Reynolds stress tensor throughout a whirling annular seal are presented. The data was collected with a three dimensional laser Doppler velocimeter using phase averaging. Two axial flow conditions (Re=12,000 and 24,000) were studied at one shaft speed (Ta=6,600). The eccentricity and whirl ratios were 50% and 100%, respectively. There is a region of high axial momentum at the inlet on the pressure side of the clearance that migrates around the seal to the suction side at the exit. The normalized axial momentum in this region is higher in the low Reynolds number case due to an axial recirculation zone that occurs on the suction side of the rotor at the inlet. The recirculation zone does not occur in the high Reynolds number case. At both Reynolds numbers there is a recirculation zone on the rotor surface in the pressure side of the inlet. This recirculation zone extends from 20° to 200° past the rotor zenith in the tangential direction, and is one third of a clearance wide radially. The high Reynolds number recirculation zone is 1.5 mean clearances long, while the low Reynolds number zone extends 2 mean clearances downstream. When compared to previous studies, it is apparent that the tangential momentum is no greater for a seal with whirl than for one without if other parameters are constant. Areas of high tangential momentum occur in the clearance where the axial momentum is low. Average exit plane tangential velocities in the high Reynolds number case are 1.5 times greater than those in the other flow case. These results are in general agreement with predictions made by other investigators.

INTRODUCTION

Annular seals control leakage from high to low pressure areas in pumps, compressors and other turbomachines operating at high speeds. A secondary but equally important purpose is to provide rotordynamic stability (Tam et al., 1988). The seal separates high pressure from low pressure regions, but some leakage is desirable, providing damping for the vibrating system, cooling on the shaft, and increasing stability. Seals with a small axial Reynolds number (generally below 2000) are generally unstable while seals with large axial Reynolds numbers produce large damping and stiffness coefficients and therefore contribute to stability (Allaire et al., 1978).

The mechanical performance of an annular seal is implicitly dependent on the fluid flow through the clearance, since the forces in the seal are generated hydrodynamically. Destabilizing forces tend to move the rotor of an annular seal from its centered position, and whirl usually follows. Whirl occurs when the center of the rotor precesses around the center of the stator. The whirl ratio is defined as $\omega=\omega_p/\omega_r$. The rotor excitation can become so great that the rotor will contact the stator.

There is usually much effort devoted to characterizing and predicting the damping, stiffness and inertia variables in a seal to decide whether it will be stable prior to production. While the macroscopic effects have been studied extensively, the flow field within the seal has not been investigated because of the difficulty of the measurement. The clearances must be very small to simulate a real machine, and it is very difficult to measure velocities in the wake of the rotor.

Previous Research Annular seals have been investigated since the mid 1970's, when they were identified as contributors to turbomachine instabilities. In 1977 data became available for a wide range of operating conditions because of research directed toward the fuel pumps in the Space Shuttle's main engine (Tam, 1988). The following is a review of some relevant research regarding fluid flow through eccentric annular seals. The investigations mainly involved rotordynamic modeling, but one effort was directed wholly to measuring the flow field in an annular seal.

Lessen (1987) performed an analytical study of the flow in a dynamically eccentric whirling annular seal at an arbitrary Taylor number within the Taylor vortex regime. Axial flow through the seal was modeled as plug flow which was justified by assuming high momentum transport from Taylor vortices. Boundary layers near the rotor and stator surface were dominated by Goertler disturbances (instabilities akin to Tollmein-Schlichting waves). Goertler disturbances were induced by the curvature of the boundary surface, and in this geometry are of far less importance than the Taylor vortices (Schlichting, 1979). The width of the Goertler disturbance-dominated regime was taken to be one unit of the non-dimensional Blasius variable, $y\sqrt{U/\nu x}$, at which point the local velocity u/U_{sve} was 0.33. Lessen suggests that marginally unstable Goertler disturbances will be superseded by Tollmein-Schlichting waves if the sum of squared axial and tangential Reynolds numbers exceeds the critical Reynolds number for their formation: $Re_x^2+Re_\theta^2 \geq Re_{crit}^2$. This indicates that the nature of the turbulence in the seal resembles flat plate turbulence at high tangential and axial Reynolds numbers. It was further found that the reaction forces in the radial direction were inertial in nature and could induce instabilities, and that the tangential reaction force was purely a function of viscous forces. Finally the ratio of potential core circulation to shaft circulation was the same in the eccentric rotor case as in the concentric. Lessen's important finding was that tangential flow circulation did not change when the rotor was offset eccentrically (whirl was not considered).

---

[1]This work was performed under NAG3-181 with the NASA Lewis Research Center and the Texas A&M University Turbomachinery Laboratory Research Consortium.

Chen and Jackson (1984) studied the effect of axial eccentricity (displacement in the r-θ plane) and misalignment (angular displacement in the Z-r plane) on rotordynamic coefficients in annular seals. They suggested that the forces generated in high pressure seals are greatest in straight annular seals, and developed relationships between reaction forces and leakage rate through the seals that included the effects of eccentricity, misalignment and rotation. A concentric tapered annular seal was used as a model for the eccentric seal, and it was found that the effect of eccentricity or misalignment on the leakage rate was not as great when the flow regime was turbulent. The seal leakage increased with the degree of eccentricity, and decreased with the degree of misalignment.

Allaire et al. (1978) obtained an analytical solution of the semi-empirical bulk flow equations developed by Hirs (1978) for pressure in an eccentric non-rotating annular seal. The seal length-to-diameter ratio was 0.16 and the axial Reynolds number was about an order of magnitude larger than the tangential. He found that in seals with a small axial Reynolds number the pressure drop though the seal was mainly due to friction effects, but as the leakage rate increased the Bernoulli effect became stronger and high pressure gradients existed through the seal. At very high flow rates, large head losses occurred at the entrance to the seal and the pressure distribution throughout the seal tended to be constant. The load-carrying capacity of the seal was small for the low flow rate case, increased as the flow rate increased, peaked where the pressure gradients were high, and then decreased as the flow rate increased.

Hashimoto et al. (1988) investigated short, eccentric journal bearings to find the effect of fluid inertia on trajectory. This was basically an investigation of whether laminar flow theory would suffice in turbulent conditions. The length-to-diameter ratio of the journal was 0.5. The averaged form of the momentum and continuity equations was used in the analysis and reaction forces were calculated for the fluctuating pressure term. Through numerical simulation the trajectory of the journals was calculated and it was demonstrated that fluid inertial effects help contribute to the stability of the system.

Kanemori and Iwatsubo (1989) considered a long annular seal with a length-to-diameter ratio of 3.0. The eccentricity of the shaft was adjustable and misalignment was not considered. They concluded that for small axial flow rates the results were similar to predictions from Fritz's theory. This did not consider the axial flow and simply suggested that the reaction force in the seal was dependent on the whirl velocity. It was determined that the tangential reaction force was destabilizing for whirl ratios between zero and 1/2, and that the seal was unstable at small Re_z, but stable at higher Reynolds numbers. The amplitude of the tangential reaction force was minimized when the whirl ratio was 1/2.

Simon and Frene (1989) studied convergent and divergent annular seals with a cryogenic working fluid. They considered the compressibility and variable viscosity of the fluid, inlet swirl and pressure drop effects. The initial assumption was that inertial effects of the fluid in the seal could be neglected. A numerical example was run with axial Reynolds numbers about 130,000 and 160,000. This example indicated the utility of the variation of the fluid properties in the analysis. Their results were in good agreement with experimental data.

Tam et al. (1988) conducted a numerical study of eccentric annular seals without misalignment, using a model of the fluid forces based on the average fluid circumferential velocity ratio. The model was based on the assumption that the dynamic forces were rotating at the precession speed. The numerical grid was three dimensional and rotated with respect to a stationary observer at the precession rate of the rotor, i.e. the rotor was a stationary reference frame. The grid consisted of 12x6x16 cells in the tangential, radial, and axial directions, and was considered invariant in time since the orbit was circular and periodic. The Prandtl mixing length turbulence model was selected because of its simplicity and because the mixing length was obviously the clearance of the seal. The eddy viscosity concept, $\mu_t=\rho l^2_m\phi$, was used to simulate the effect of the turbulence levels on the mean velocities. The pressure drops ranged from 0.3 to 18.5 bars, the rotational shaft speeds from 1442 to 5085 rpm, the eccentricity ratios from 0.24 to 0.8, and the whirl ratios from 0.3 to 1.0. Bromotriflouromethane and oil were modeled as the working fluids.

The results of the study indicated that there were significant changes in the local values of the seal dynamic forces and that large tangential separation zones existed through the seal. The existence of the recirculation zones was found to depend on the shaft and precession speeds, with increasing likelihood at lower shaft speeds and higher precession speeds (whirl ratio approaching 1.0). Recirculation zones were located along the stator wall, beginning just prior to the minimum clearance location, and rotated at the precession speed. Negative preswirl (opposing the direction of seal rotation) intensified the recirculation zones while preswirl in the direction of rotation weakened the secondary flow.

The effects of eccentricity and rotation speed on leakage flow rate were also studied. Leakage was most dependent on rotational speed when the precession speed was low. Increasing precession speed increased the leakage rate through the seal because of a pumping effect.

Fluid injection from four stator positions into the clearance was also studied. It was found that injection in the direction of the shaft rotation increased leakage while injection against the rotation decreased leakage. Injection essentially mimicked the preswirl effects mentioned earlier, but downstream of the inlet.

Johnson (1989) and Morrison et al. (1991) used a three dimensional laser Doppler anemometer to study an annular seal positioned first concentrically and then eccentrically. The eccentricity was created by moving the stator closer to the rotor at an angular position of interest (the rotor was not whirling). Johnson measured axial-radial profiles at θ=0°, 90°, 180°, and 270°. The leakage flow was 4.86 l/s (77 gpm, Re=24,000) and the rotational speed varied from 0 to 3600 rpm(Ta = 0 to 6,600). The preswirl was 0°, -45°, and +45°.

For the rotor concentric with the stator, tangential velocities were higher ($\approx$0.3 W_{sh}) for positive preswirl than for no preswirl ($\approx$0.18W_{sh}) or negative preswirl (-0.25W_{sh} at the inlet and 0.10W_{sh} at the exit). For the eccentrically mounted stator, tangential velocities vary to satisfy continuity considerations being greater in the small clearance than in the large. In the large clearance the tangential velocity did not increase along the length of the seal but in the small clearance there was azimuthal acceleration. The effect of preswirl was similar to that for the concentric geometry.

In summary, previous studies showed that eccentrically aligned rotors affect annular seals in several ways. The core circulation in an eccentric seal is the same as in concentric seals (Lessen, 1987). Whirling rotors increase the leakage flow rate through seals, presumably due to a pumping effect (Chen and Jackson, 1984 and Tam, 1988). High leakage rates through the seal decrease the axial pressure gradient across the rotor because of high head losses in the entrance region (Allaire, 1978). High turbulence levels enhance the stability of whirling journals, suggesting that once whirling begins it may be damped out (Hashimoto et al., 1988). Seals are unstable at

low axial Reynolds numbers (below 2000) (Allaire et al. 1978 and Kanemori and Iwatsubo, 1989). Reaction forces are destabilizing when the whirl ratio is less than 0.5 (Kanemori and Iwatsubo, 1989). Tangential recirculation zones discovered in whirling seals during certain operating conditions were seen to diminish if there was preswirl or fluid injection in the direction of rotor rotation, and were enhanced if preswirl or injection opposed the rotor circulation direction (Tam, 1988). Morrison, et al. (1991) and Johnson (1989) showed that preswirl effects tangential velocity development in concentric and statically eccentric seals.

Measuring the velocity profile in the whirling seal is the only means to test the validity of assumptions used in the analysis of other researchers. For example, it is highly unlikely that the axial velocity distribution in the seal can be modeled as a plug flow as hypothesized by Lessen. Theories that were proposed in these studies and tested include the proposition that 1) the tangential velocity distribution does not increase in the presence of whirl, 2) there is a tangential velocity recirculation zone along the stator, and 3) that seal leakage increases with eccentricity.

PROGRAM OBJECTIVES

To address the lack of experimental data, the mean velocity profile and turbulence levels in an annular seal (37.3 mm long, 164.1 mm diameter, and a nominal clearance of 1.27 mm) were measured for evaluation of flow phenomena. Figure 1 illustrates the test section in which water is the working fluid. The stator contains an optical window through which the beams of a three-dimensional laser Doppler velocimeter are directed. An eccentricity ratio of 0.5 is imposed on the rotor by mounting it on an eccentric bushing, which is attached to the shaft of an electric motor (the eccentricity ratio is defined as the ratio of the off-centeredness of the rotor to the clearance width, $\epsilon = e/c$). A detailed description of the facility and error analysis are contained in Johnson (1989) and Morrison, et al.(1991). In real machines eccentricities can be attributed to misalignment during assembly, side loads such as rotor weight, impeller loads (Nelson and Nguyen, 1988), or destabilizing seal forces. Instabilities caused by pressure fluctuations in the flow can also induce eccentric whirling.

By varying the flow rate through the seals, Reynolds numbers and Taylor numbers typical of full scale applications were obtained. The seal angular speed was 3600 rpm for all the tests. The leakage flow rates were 2.43 l/s (38.5 gpm) and 4.86 l/s (77 gpm), with an eccentricity ratio of 50%. Since the rotor was connected directly to the shaft of the motor, the whirl ratio was 100%. The Reynolds numbers investigated were 12,000 (U_{ave}=3.7 m/s) for the first flow case and 24,000 (U_{ave}=7.4 m/s) for the second, while the Taylor number for both cases was 6,600 (W_{sh}=28.7 m/s).

RESULTS

The rotor is spinning clockwise and whirling in the same direction as it is rotating. Angles are measured from the minimum clearance point in a clockwise direction, and the minimum clearance point is the rotor's zenith. The suction side of the clearance is on the left of the rotor, and the pressure side is on the right.

Re=12,000

Mean Velocities Significant features of the mean velocity profiles are that the axial velocity peaks on the pressure side of the clearance at the seal entrance and rotates around the seal circumferentially until it is on the suction side at the exit. The radial velocity distribution generally points outward to the stator at the seal inlet, and dissipates downstream. An axial vena contracta exists over the first two clearances on the pressure side of the rotor.

Figures 2 and 3 present contours for the three mean velocity components and the axial velocity variance. Figure 2 represents the flow at five axial locations along the entire length of the seal while Figure 3 presents data from -0.02 to 0.14 Z/L of the flow. Upstream of the inlet (Figure 3) the flow is very sensitive to the motion of the rotor, as indicated by the large radial velocities away from the rotor where it accelerates toward the stator. On the pressure side of the seal there are large tangential velocities and very small radial velocities. The large radial velocity zone is explained partially by the flow in the plenum upstream of the seal moving with the rotor from top to bottom. The rotor is pulling the flow along with it for angles larger than 180° and pushing flow away from it for angles less than 180°. Once the flow enters the seal clearance, the high radial velocities at 90° diminish and the flow follows the movements of the rotor more closely. At the inlet the $\partial/\partial\theta$ gradients are most apparent. No tangential recirculation zones were seen along the stator in this flow case; therefore, if one exists it must be between the stator and the first radial grid line.

Upstream of the inlet to the seal, at Z/L=-0.02 (Figure 3), the maximum axial velocity ($1.3U_{ave}$ where U_{ave}=3.7 m/s) occurs +95° from the rotor zenith (θ=0° position). There is a negative zone of axial velocity on the other side of the seal which reaches $-0.4U_{ave}$ (1.5 m/s). It is evident that at this location the rotor is affecting even the flow upstream of the seal. The radial flow component is moving very quickly away from the rotor ($0.9U_{ave}$=3.3 m/s) from about θ=90° to 180°, but is depressed everywhere else. This is representative of the motion of the rotor, which is pulling fluid toward it in the lower half of the stator, and pushing it away on the other side. The tangential flow component is uniformly distributed around the clearance at $0.12W_{sh}$ (W_{sh} is the rotor surface velocity, 28.7 m/s), which is on the order of U. The inlet preswirl is caused by the rotation of the rotor which influences the upstream velocities through the large volume of water trapped in the hollow section of the rotor. The tangential velocity is accelerated into the minimum clearance area beginning at 260°. To satisfy continuity, the axial or radial velocities must be reduced. Consequently, the negative axial zone begins at 260° also, but the radial velocities do not seem to react.

At the entrance, Z/L=0 (Figures 2 and 3), the maximum axial velocity increases to $2.4U_{ave}$ (8.9 m/s) and the peak location moves to 70°. The size of the back flow area diminishes, but it does not move relative to its previous position. It appears that the peak axial velocity is located in a region of decelerating tangential flow. For equal axial pressure drop across the seal at all azimuthal angles, the greatest axial velocity should be in the largest clearance area if there is no rotation or whirl. But, the tangential component accelerates toward the minimum clearance area, so the axial momentum decreases to satisfy continuity. The smallest tangential velocities

occur in a band from 60° to 230°, where the largest axial velocities are located. The greatest radial velocities continue to occur between 90° and 180°, and the maximum radial velocity is still $0.9U_{ave}$ (3.3 m/s) outward.

The axial velocity component accelerates down the seal, and the peak begins to rotate further away from the rotor zenith at Z/L=0.04 (Figure 3). The maximum axial velocity reaches $2.6U_{ave}$ (9.6 m/s) and rotates to 90° as the tangential momentum transports the large axial momentum zone around the seal. At the same time, an axial recirculation zone (due to the vena contracta effect at the seal entrance) extends around the rotor, from 80° to 320° on the rotor surface. The shear layer between the positive and negative axial velocities develops intensely at 130°, and the large axial velocities progress outward from the rotor toward the stator side of the clearance. The tangential velocities begin to increase also, especially on the suction side of the seal, where there is little axial momentum. The radial velocities clearly define the vena contracta region on the pressure side of the clearance, a strong counter flow exists at the rotor surface (≈350° to 180°) with a positive radial velocity further into the clearance. The large positive radial velocity zone has moved around the seal slightly to 300°. There are large $\partial V/\partial r$ gradients in the shear layer region around the axial recirculation zone and through the vena contracta shear layers.13

Farther down the seal, at Z/L=0.07 (Figure 3), the U component begins to drop in magnitude, with a peak velocity of $2.1U_{ave}$ (7.8 m/s) at θ=80°. The recirculation at 180° on the bottom of the rotor decreases in magnitude, and the recirculation on the opposite side of the rotor from the maximum velocity region subsides as well. The large U zone begins to spread out around the seal, and is located out closer to the stator than the rotor. Large $\overline{u'u'}$ stresses along the rotor surface divert the flow out to the stator. The radial velocities are directed into the rotor in much of the zone occupied by the high axial velocities, but are positive in the U recirculation areas. The W distribution is more uniform, at $0.20W_{sh}$ (5.7 m/s) throughout much of the seal. The tangential velocity contours are closer together in the small clearance area of the seal, but they are still evenly distributed throughout the clearance. It appears that the $\partial W/\partial r$ gradients scale with the clearance width.

Between Z/L=0.07 and 0.21 the peak axial velocity decreases and spreads over a much greater area of the clearance as the flow continues downstream. The deceleration is due to shear along the stator wall and conservation of momentum, since the high axial flow area is spread out over more of the seal. This is the region where the vena contracta diverges out to reattach to the rotor surface, and the axial recirculation disappears. The steep $\partial V/\partial r$ gradients toward the rotor have also diminished at this point. The positive and negative radial velocity zones begin to equalize on either side of the seal and approach zero.

At the midplane of the seal (Z/L=0.50, Figure 2) the U profile becomes almost uniformly distributed, with a peak of $1.1U_{ave}$ (4 m/s) at θ=135°. The $0.8U_{ave}$ (3 m/s) contour extends throughout most of the circumference of the seal. The radial velocities are virtually zero throughout the entire seal, and the tangential velocities remain very uniformly distributed at an average of $0.20W_{sh}$ (5.7 m/s).

Down the seal at Z/L=0.77 a radical shift in the axial velocities occurs. The peak velocity increases to $1.5U_{ave}$ (5.5 m/s) and rotates around to θ=295°. The axial recirculation does not reappear, and the peak velocity is fairly close to the rotor, indicating that there are low turbulence levels there. The positive and negative radial velocity zones have also rotated to opposite sides of the seal, with the negative areas following the peak axial velocity zone. The magnitude of the radial velocities is below $0.05U_{ave}$ (0.18 m/s). The tangential profile shifts with the larger tangential velocities located in the pressure side of the seal, which is consistent with the downstream trend that large tangential velocities belie small axial velocities, and vice versa.

The axial velocity profile continues to change all the way to the exit plane (Z/L=1.00) with the peak axial velocity progressing toward the rotor zenith. The radial velocities are similar at Z/L = 0.77 and 1.00. At the exit, tangential velocities reach a maximum across the width of the clearance with high tangential velocities extending from the pressure side of the seal at θ=60° to the suction side at θ=200° at values near $0.3W_{sh}$ (8.6 m/s or $2.3U_{ave}$).

Turbulence Levels Upstream of the inlet to the seal the $\overline{u'u'}$ Reynolds stress is evenly distributed throughout the clearance averaging $0.1U_{ave}^2$ (Figure 3, 1.4 m^2/s^2). This stress level is what remains of the grid turbulence generated at the entrance to the plenum. At the inlet, the normal stresses begin building up, thereby inhibiting the flow along the rotor. The $\overline{u'u'}$ stress increases sharply along the rotor from 45° to 175°, and the $\partial\overline{u'u'}/\partial r$ gradients are very large halfway into the clearance. This normal stress, which is analogous to a pressure (Rodi, 1984), retards the axial flow along the rotor. Similarly, gradients of the normal stress are considered as dynamic pressure gradients (Tennekes and Lumley, 1990). The high "pressure" area blocks axial flow along the rotor, diverts it up into the vena contracta, and induces recirculation behind it. Downstream of the inlet at Z/L=0.04 (Figure 3), the $\overline{u'u'}$ stresses reach a maximum of $0.9U^2$ (12 m^2/s^2)at 70°. The peak is located a quarter clearance from the rotor, begins developing at 310°, builds to a maximum at 70°, then diminishes to a minimum at 300°. The $\partial\overline{u'u'}/\partial r$ gradients between the $\overline{u'u'}$ peak and the U peak are very steep in the shear layers along the recirculation zone. Three quarters of the clearance from the rotor and at 80° the $\overline{u'u'}$ stresses recede to $0.2U_{ave}^2$, and the U velocity reaches a maximum. This location is where the vena contracta reaches its narrowest width. The $\partial\overline{u'u'}/\partial\theta$ gradients are greater on the upstream side of the peak and then trail off at a gentler slope downstream. At Z/L=0.07 the $\overline{u'u'}$ stress is convected tangentially around the seal to 80° from 70° just upstream. The structure is still intact but the gradients are smaller than before. The peak is still dropping, reaching $0.7U^2$ (9.5 m^2/s^2) at 80°. The $\overline{u'u'}$ stresses dissipate rapidly between Z/L=0.07 and Z/L=0.21. The peak level convected to 100°, so the convection of the $\overline{u'u'}$ stress increases also. The $\overline{u'u'}$ gradients in both the axial and tangential directions decrease in magnitude. At Z/L=0.21 the $\overline{u'u'}$ normal stress is distributed across the entire clearance on the pressure side of the rotor. This reduces the mean velocity peak, whereas before the high $\overline{u'u'}$ levels on the rotor surface had pushed the high U velocities toward the stator. At the midplane of the seal (Z/L=0.50) the $\overline{u'u'}$ stresses stop changing any further. The peak $\overline{u'u'}$ stress is $0.15U_{ave}^2$ (2 m^2/s^2), and it is located in a bubble on the bottom of the rotor where the recirculation was located nearer to the inlet. Another bubble develops in the minimum clearance area. For the rest of the seal these structures change little, suggesting that production and dissipation are in equilibrium from this point on.

Re=24,000

Mean Velocities The mean velocity contour plots reveal an interesting change in the upstream flow patterns with the increased flow rate through the seal. Upstream and at the inlet to the seal (Figures 4 and 5) the flow vectors on the pressure side are pointing inward, as

opposed to outward as they did in the slower flow rate. Upstream of the seal at Z/L=-0.02 (Figure 5), the mean axial velocity profile reaches a peak of greater than $0.9U_{ave}$ (6.6 m/s, where U_{ave}=7.4 m/s) between 60° and 135°. There is no backflow out of the seal as in the lower Reynolds number case because the upstream pressure is higher, and the pressure developed in the seal cannot overcome it. The radial velocities are generally pointed inward toward the seal as the flow has just been diverted inward by the curve in the plenum wall. The greatest inward mean radial velocities are located in the same region as the high U's. There is much less significant preswirl at the inlet for this case. The inlet W does not exceed $0.08W_{sh}$ ($0.33U_{ave}$, 2.4 m/s) over most of the clearance.

At the seal inlet (Figure 4) the axial flow component begins accelerating into the seal. The peak axial velocity is $1.5U_{ave}$ (11 m/s) across a band from 30° to 60° and stays above $0.5U_{ave}$ (3.7 m/s) across the entire circumference of the seal. The V profiles continue the strong inward trend. The maximum inward velocity reaches $-0.8U_{ave}$ (-6 m/s) from 45° to 190°. It appears that the inward momentum imparted to the flow by the curved stator wall is still affecting the fluid, but at the same time the inlet shape of the seal is directing flow to the cavity under the seal. The tangential velocities begin to increase, with the $0.08W_{sh}$ (2.4 m/s) contour extending almost to the stator from 280° to 60°, and moving outward through the suction portion of the clearance.

Just downstream of the inlet at Z/L=0.04 (Figure 5) the axial velocities are much greater, with a maximum of $2.2U_{ave}$ (16.3 m/s) occurring at 95°. This peak is very close to the stator, and there are very high $\partial U/\partial r$ gradients on either side of the peak. A shear layer exists from 90° to 180° and stretches away from the rotor on the maximum clearance side. A mild recirculation zone exists between the rotor and the shear layer with a maximum backflow velocity of $0.1U_{ave}$ (-0.7 m/s). This recirculation zone occupies less than 15% of the clearance and is not visible on the figures. Reattachment of the axial velocity occurs at 180° where the axial velocities are significantly smaller than on the other side of the clearance. The axial recirculation produces a small vena contracta similar to that for the low Reynolds number case but much smaller in magnitude. The V profile changes significantly at this point, as the direction of the velocities is redirected back out toward the stator. A maximum of $0.18U_{ave}$ (1.3 m/s) at 45° is surrounded by mild $\partial V/\partial r$ gradients on either side. The radial velocities are pointed outward near the rotor and inward near the stator on the wide clearance side of the rotor, indicating the presence of a vena contracta around 135°. Because the axial momentum in this area is so small, the tangential velocities are able to develop quickly, especially in the recirculation zone where $W=0.24W_{sh}$ (6.9 m/s, $0.9U_{ave}$) in the middle of the clearance from 60° to 280°.

From Z/L=0.04 to Z/L=0.07 (Figure 5) the axial velocities decrease, only reaching a maximum of $1.9U_{ave}$ (14 m/s) at θ=120°. The high velocity area is still along the stator, and the steep $\partial U/\partial r$ gradients near the rotor surface are relaxing. The recirculation zone has disappeared along the rotor, but the velocities are still very low there. The disappearance of the shear layer implies that the axial streamlines are reattached to the rotor. The radial velocities are directed back out toward the stator after turning at the reattachment point. The tangential velocity development diminished with the reattachment of the axial velocity streamlines.

Moving to Z/L=0.14 (Figure 5), the U profile is more evenly distributed throughout more of the seal, as the peak axial momentum region reaches wider clearances, which is decelerating the flow. The peak axial velocity is $1.5U_{ave}$ (11 m/s) and it is located at 90°. The rest of the profile remains attached to the rotor and stator with very mild $\partial U/\partial r$ gradients. The axial velocity on the suction side of the rotor is steadily increasing, with the minimum continuous contour at $0.7U_{ave}$, where just upstream it is $0.6U_{ave}$. The radial velocities continue to decrease in magnitude and now are fairly insignificant. The decrease in axial momentum is acting favorably for the tangential velocities, which are now increasing over the entire seal. The $0.08W_{sh}$ (2.4 m/s) level is now extending much further into the maximum clearance region, and it is distributed more uniformly.

From Z/L=0.14 to Z/L=0.50 (Figure 4) the trends discussed above continue; the axial velocity continues to spread more uniformly across the entire seal, the radial velocities remain small, and the tangential velocities increase with the decrease in axial momentum. At the midplane the axial profile is almost uniform, with regions in the maximum clearance region having velocities which are a little higher. As the location of the maximum axial velocity rotates around the seal, the negative radial velocity zone also moves. By the midplane it is relocated to the minimum clearance region. The tangential velocity develops to $0.08W_{sh}$ all the way out to the stator, and it is increasing in the pressure section of the clearance, reaching $0.16W_{sh}$ (4.8 m/s) by the midplane.

Farther down the seal at Z/L=0.77 the location of the maximum axial velocity is convected around the seal by the increasing tangential velocity component. The peak axial velocity is at 240° and has increased to $1.4U_{ave}$ (10.4 m/s) as the tangential component is forcing the fluid into a smaller region. The radial velocity is similar to that upstream, with positive values pointing out from the rotor and negative in from the stator. The tangential profile develops significantly, with the $0.24W_{sh}$ (6.9 m/s) zone extending almost entirely across the pressure zone around 60°. This significant increase in the tangential momentum is the mechanism driving the axial velocity peak around to the other side of the clearance.

The axial velocities on the suction side of the clearance continue to increase as the flow progresses downstream while the tangential velocities increase on the pressure side. This continues to the exit plane where the peak axial velocity reaches $1.7U_{ave}$ (12.6 m/s) at 265°. At the exit plane nearly the whole pressure side of the clearance is dominated by tangential velocities of at least $0.24W_{sh}$ (0.93U) and on the suction side they are $0.16W_{sh}$ (4.6 m/s). The radial profile remains virtually unchanged through the rest of the seal, not exceeding $0.08U_{ave}$ (0.6 m/s). The radial velocities are pointed inward along the stator.

Turbulence Levels Upstream of the inlet, in the plenum at Z/L=-0.02 (Figure 5), the normal Reynolds stress term is extremely subdued, which is reflected in the mild gradients in the mean velocity terms. The $\overline{u'u'}$ term barely reaches more than $0.05U_{ave}^2$ (2.7 m^2/s^2). At the inlet (Figure 4) the front edge of the rotor causes changes. The $\overline{u'u'}$ term builds (exceeding $0.33U_{ave}^2$, 18 m^2/s^2)along the rotor surface on the bottom side where the recirculation zone is located a bit farther downstream. (Note: the recirculation is evident in the numerical data but does not appear in the contour plots.) This stress decelerates the axial velocity at the surface of the rotor. By Z/L=0.07 (Figure 5), the $\overline{u'u'}$ value decreases with the large gradients also showing a marked reduction. The peak of the $\overline{u'u'}$ stress is transported to 110° by the tangential momentum, and the peak has diminished. Dissipation dominates the flow at this point, where upstream turbulence production is the major mechanism, and works to distribute the turbulence term fairly evenly by midplane. The profile remains reasonably uniform on the suction side, but by the exit plane, Z/L=1.00, there are again high values of $\overline{u'u'}$. Although the gradients are steep, it seems likely that the phenomenon is real because of the circumference over which it is distributed. The turbulence producing source at this plane is the step at the end of the seal.

SUMMARY

The flow field inside an annular seal whirling at a whirl ratio of 1 and an eccentricity ratio of 0.50 has been measured using a 3-D laser Doppler anemometer system. Reynolds numbers of 12,000 and 24,000 were investigated while the Taylor number was held constant at 6,600. The flow structure, as evidenced by the velocity and turbulence distributions in the whirling annular seal proved to be far different than in a statically eccentric seal otherwise operating at the same conditions. Prominent features included a peak axial velocity that began in the pressure section of the clearance at the inlet and rotated around to the suction side of the clearance at the exit, a vena contracta on the pressure side of the rotor, and no significant increase in tangential velocity with whirling rotor motion when compared to statically eccentric seals.

The axial flow profiles for both the high and low Reynolds number cases have similarities but also display substantial differences. In both the profiles, the peak axial velocity rotates from the pressure to the suction side of the clearance. In the low Reynolds number case, this started at 60° with a magnitude of $2.4U_{ave}$ over the inlet. By midplane the profile spreads uniformly across most of the clearance. This rotates around the clearance, and at Z/L=0.77 the peak reaches the final circumferential position of 300°. Downstream of this position, the peak continues to grow, increasing to $1.9U_{ave}$ at the exit of the seal.

The mean velocity field reveals a highly three dimensional flow with large radial velocities near the inlet of the seal. The normalized axial momentum near the inlet on the pressure side of the rotor is higher in the low Reynolds number case due to an axial recirculation zone that occurs on the suction side of the rotor at the inlet. Another recirculation zone exists on the rotor surface on the pressure side of the inlet at both Reynolds numbers. This recirculation zone extends from 20° to 200° in the tangential direction, and is one third of a clearance wide radially (not apparent in the contour plots). The high Reynolds number recirculation zone is 1.5 mean clearances long, while the low Reynolds number zone extends 2 mean clearances downstream. When compared to previous non-whirling flow studies (Johnson (1989)) at similar flow parameters, the tangential momentum does not significantly increase with the onset of whirl. Areas of high tangential momentum occur in regions of the clearance where the axial momentum is low. Average exit plane tangential velocities in the low Reynolds number case are 1.5 times greater than those in the high Reynolds number case.

NOMENCLATURE

A	Leakage area, m^2
c	Mean clearance between the stator and rotor, m
d	Rotor diameter, m
e	Eccentricity, m
L	Length of the seal, m
l_m	Mixing length, m
Q	Leakage flow rate, m^3/s
r	Radial distance from stator centerline, m
Re	Reynolds number = $2Uc/\nu$
$Re_{x,\theta}$	Reynolds number in axial (x) or tangential (θ) direction
Re_{crit}	Critical Reynolds number for transition to turbulence
Ta	Taylor number = $\frac{cW_{sh}}{\nu}\sqrt{\frac{2c}{d}}$
U	Axial mean velocity, m/s
U_{ave}	Bulk mean velocity=Q/A, m/s
V	Radial mean velocity, m/s
W	Tangential mean velocity, m/s
$\overline{u'u'}$	Time averaged Reynolds stress, m^2/s^2
W_{sh}	Rotor surface speed, m/s
Z	Distance downstream of the seal inlet, m
ϵ	Eccentricity ratio, e/c
θ	Azimuthal angle measured in the direction of rotation from the minimum clearance
μ	Fluid absolute viscosity, (N s)/m^2
μ_t	Turbulent eddy viscosity, (N s)/m^2
ϕ	Strain rate
ν	Kinematic viscosity, m^2/s
ρ	Fluid density, kg/m^3
ω	Whirl ratio, ω_p/ω_r
ω_p	Rotor precession speed, rpm
ω_r	Rotor speed, rpm

BIBLIOGRAPHY

Allaire, P.E., Lee, C.C., Gunter, E.J, 1978, "Dynamics of Short Eccentric Plain Seals with High Axial Reynolds Numbers," *Journal of Spacecraft and Rockets*, Vol. 15, pp. 341-347.

Chen, W. C., and Jackson, E.D., 1984, "Eccentricity and Misalignment Effects on the Performance of High-Pressure Annular Seals," *ASLE Transactions*, Vol. 28, pp. 104-110.

Hashimoto, H., Wada, S., Sumitomo, M., 1988, "Effects of Fluid Inertia Forces on the Dynamic Behavior of Short Journal Bearings in Superlaminar Flow Regimes," *Journal of Tribology*, Vol. 110, pp. 539-547.

Hirs, G.G., 1973, "Bulk-Flow Lubricant Theory for Turbulence in Lubricant Films," *ASME Journal of Lubricant Technology*, Vol. 95, pp. 137-146.

Johnson, M.C., 1989, "Development of a 3-D Laser Doppler Anemometry System: With Measurements in Annular and Labyrinth Seals," Ph.D. Dissertation, Texas A&M University, College Station, Texas, 77843.

Kanemori, Y., and Iwatsubo, T., 1989, "Experimental Study of Dynamical Characteristics of a Long Annular Seal," *JSME International Journal Series II*, Vol. 32, pp. 218-224.

Lessen, M., 1987, "Turbulent Flow in Shaft Seals and Bearings," *STLE Tribology Transactions*, Vol. 31, pp. 390-396.

Morrison, G.L., Johnson, M.C., and Tatterson, G.B., 1991, "Three-Dimensional Laser Anemometer Measurements in an Annular Seal," *ASME Journal of Tribology*, Vol. 113, pp. 421-427.

Nelson, C.C., Nguyen, D.T., 1988, "Analysis of Eccentric Annular Incompressible Seals: Part 1-A New Solution Using Fast Fourier Transforms for Determining Hydrodynamic Force," *ASME Journal of Tribology*, Vol. 110, pp. 354-360.

Rodi, W., 1984, *Turbulence Models and Their Application in Hydraulics - A State of the Art Review*, 2nd Edition, International Association for Hydraulic Research, Rotterdam, The Netherlands.

Schlichting, H., 1979, *Boundary-Layer Theory*, McGraw-Hill Classic Textbook Reissue, New York.

Simon, F., Frene, J., 1989, "Static and Dynamic Characteristics of Turbulent Annular Eccentric Seals: Effect of Convergent-Tapered Geometry and Variable Fluid Properties," *ASME Journal of Tribology*, Vol. 111, pp. 378-385.

Tam, L.T., Przekwas, A.J., Muszynska, A., Hendriks, R.C., Braun, M.J., Mullen, R.L., 1988, "Numerical and Analytical Study of Fluid Dynamic Forces in Seals and Bearings," *Journal of Vibration, Acoustics, Stress, and Reliability in Design*, Vol. 110, pp. 315-325.

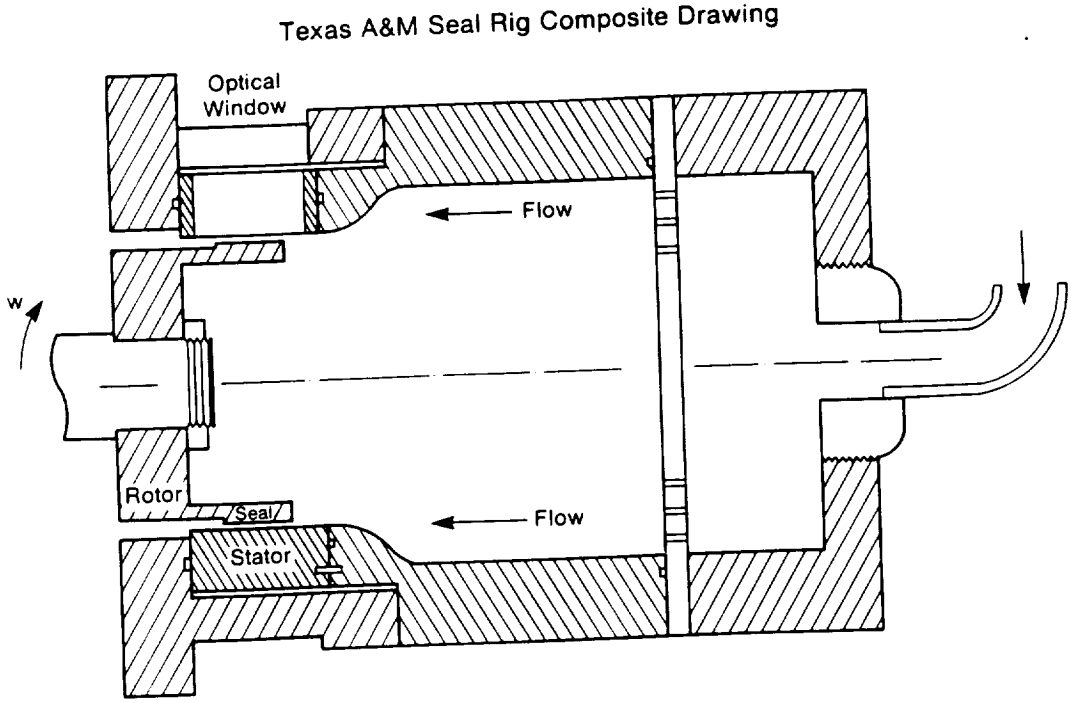

Figure 1. Annular seal test facility.

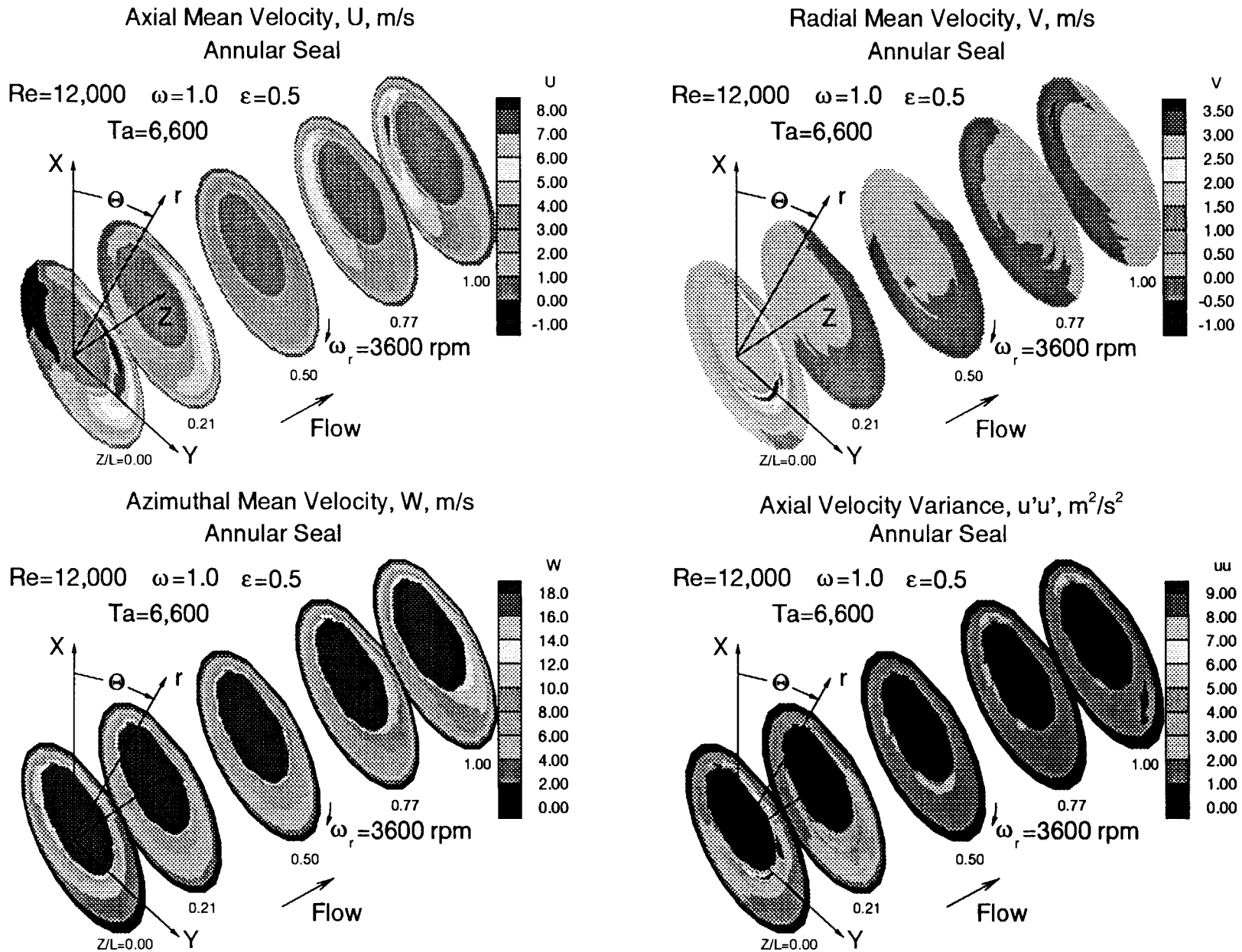

Figure 2. Mean velocity and axial velocity variance, Re=12,000, $0.00 \leq Z/L \leq 1.00$.

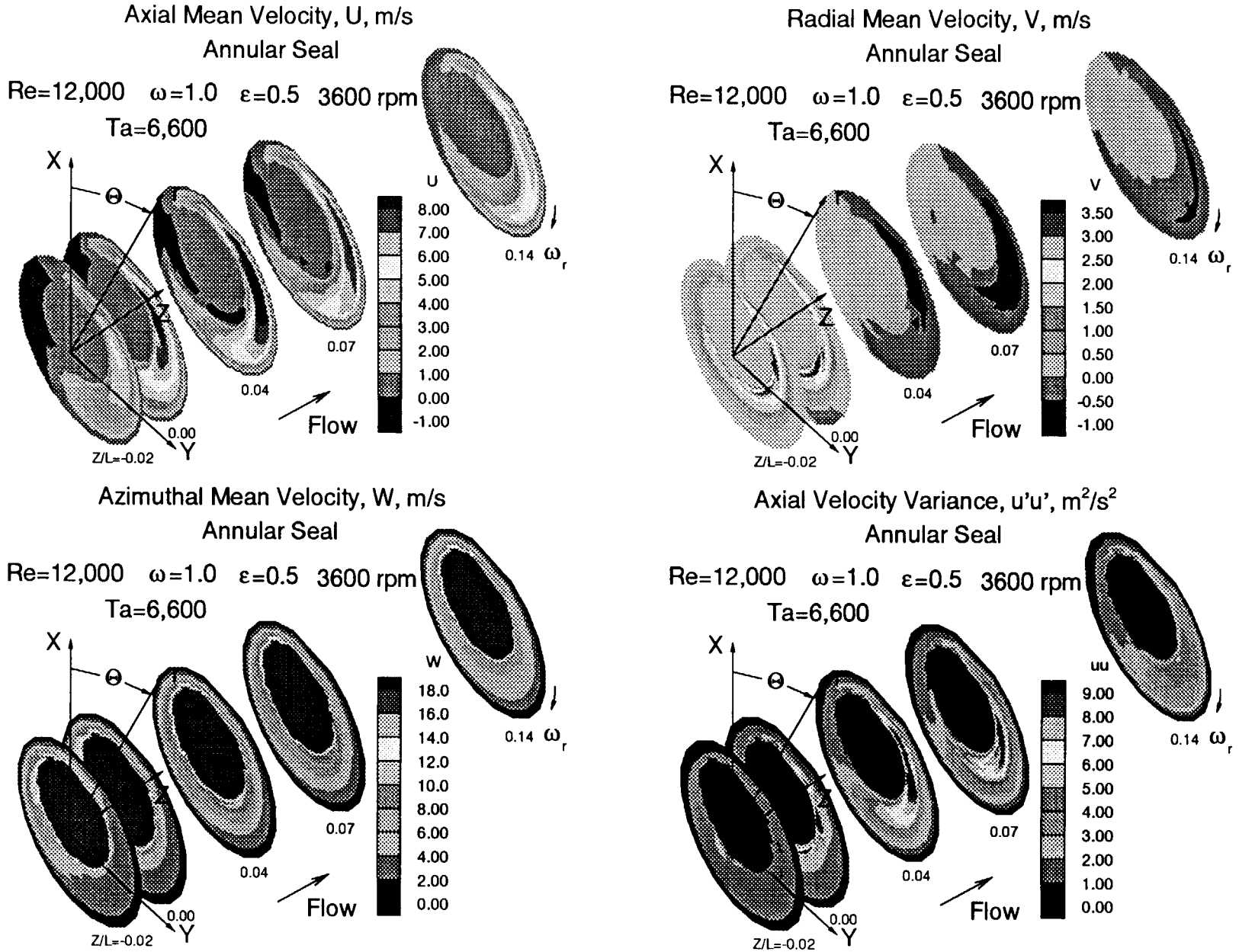

Figure 3. Mean velocity and axial velocity variance, Re=12,000, $-0.02 \leq Z/L \leq 0.14$.

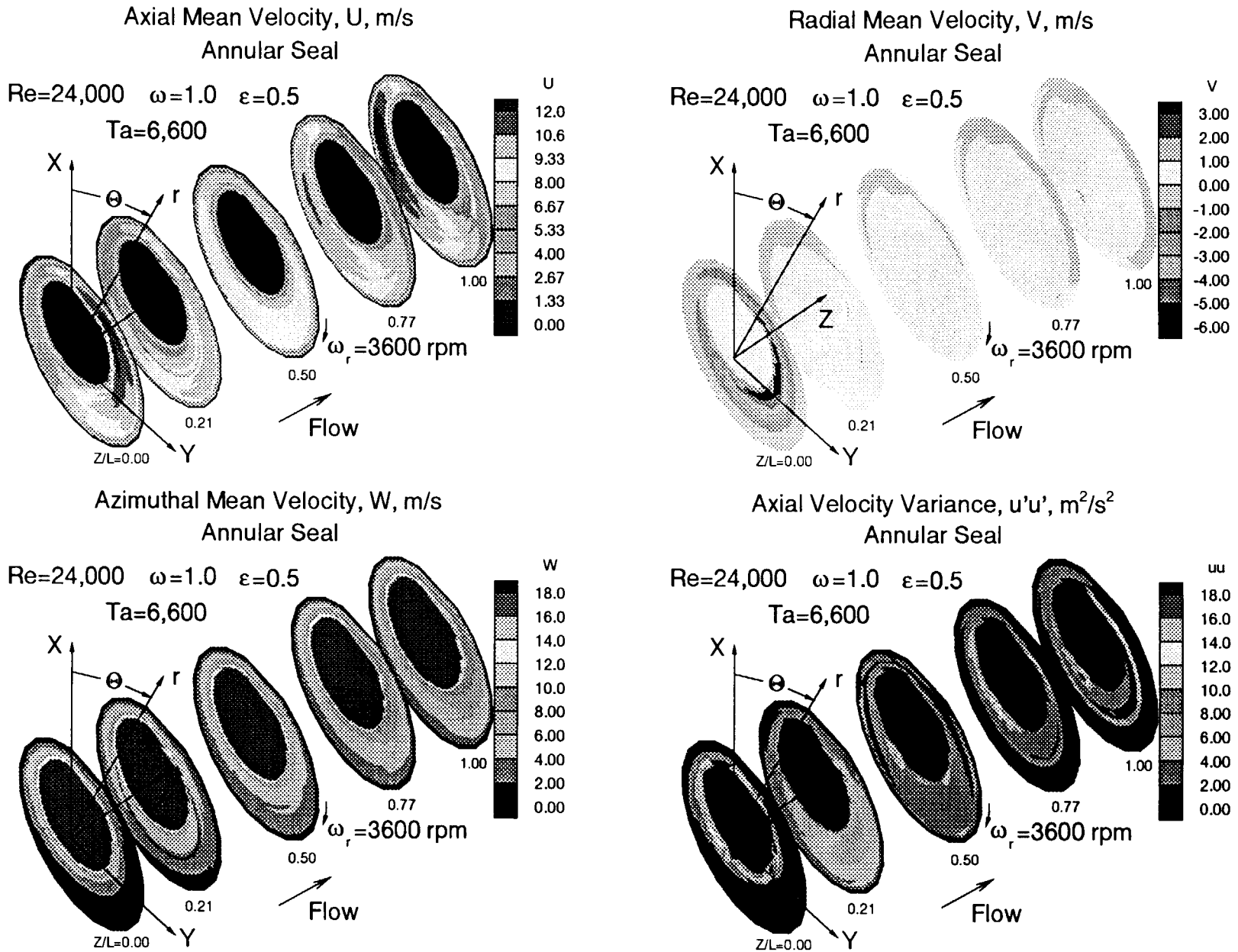

Figure 4. Mean velocity and axial velocity variance, Re=24,000, $0.00 \leq Z/L \leq 1.00$.

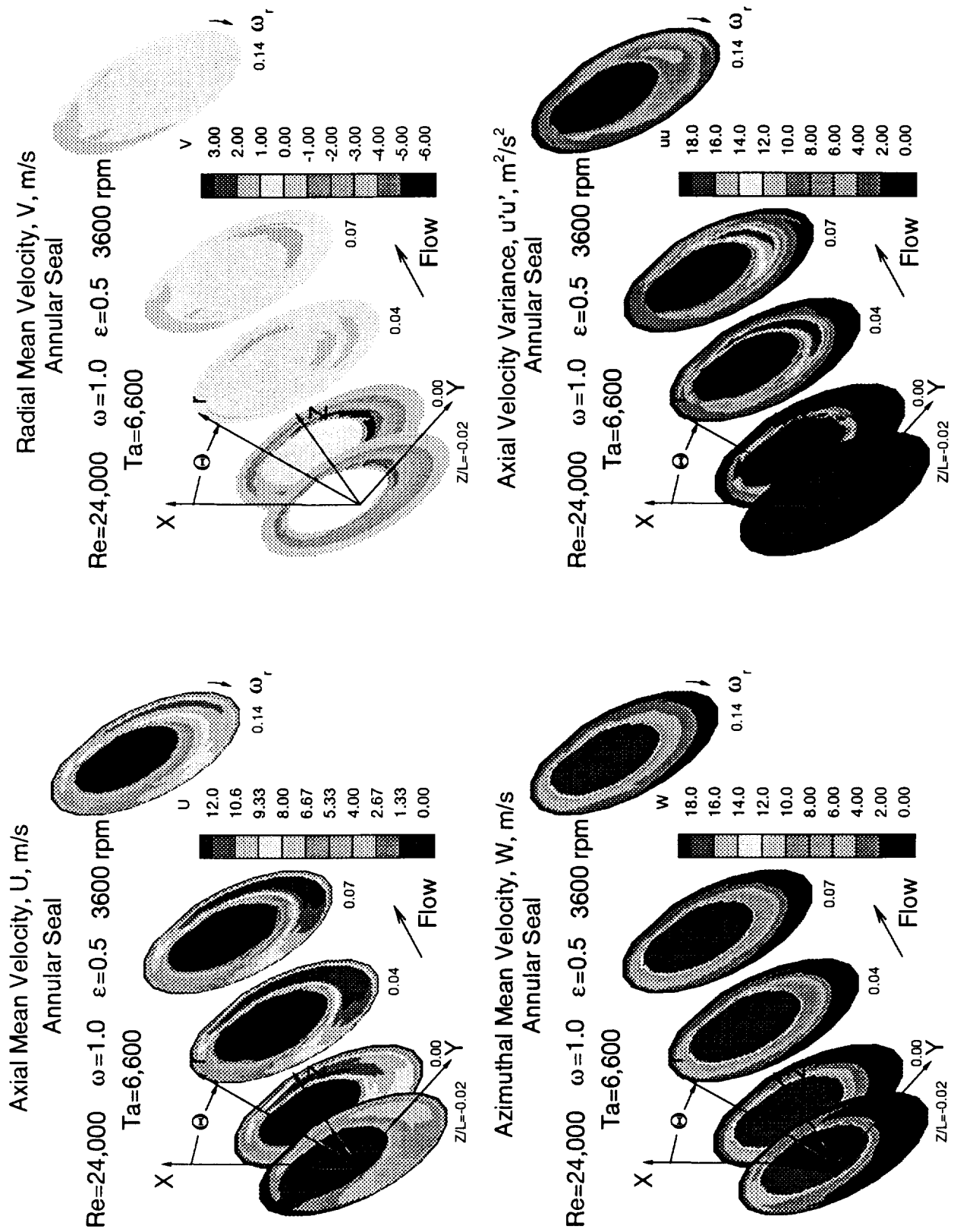

Figure 5. Mean velocity and axial velocity variance, Re=24,000, $-0.02 \leq Z/L \leq 0.14$.

An Experimental Technique For Performing 3-D LDA Measurements Inside Whirling Annular Seals

by

Gerald L. Morrison
Mark C. Johnson
Robert E. DeOtte, Jr.
H. Davis Thames III
Brian G. Wiedner
Mechanical Engineering Department
Turbomachinery Laboratory
Texas A&M University
College Station, Texas 77843

Presented at

Sixth International Symposium On Application
Of Laser Techniques To Fluid Mechanics
July 20-23, 1992
Lisbon, Portugal

An Experimental Technique For Performing 3-D LDA Measurements Inside Whirling Annular Seals

Gerald L. Morrison, Professor
Mark C. Johnson, Assistant Professor[1]
Robert E. DeOtte, Jr., Assistant Research Engineer
H. Davis Thames III, Engineer[2]
Brian G. Wiedner, Graduate Student
Mechanical Engineering Department
Turbomachinery Laboratory
Texas A&M University
College Station, Texas 77843-3123

ABSTRACT

During the last several years, the Fluid Mechanics Division of the Turbomachinery Laboratory at Texas A&M University has developed a rather unique facility with the experimental capability for measuring the flow field inside journal bearings, labyrinth seals, and annular seals. The facility consists of a specially designed 3-D LDA system which is capable of measuring the instantaneous velocity vector within 0.2 mm of a wall while the laser beams are aligned almost perpendicular to the wall. This capability was required to measure the flow field inside journal bearings, labyrinth seals, and annular seals. A detailed description of this facility along with some representative results obtained for a whirling annular seal are presented.

INTRODUCTION

The measurement of fluid velocities in small spaces (<2 mm) where the turbulence intensities are very high (>30%) and flow reversals are present is a prime application for laser anemometry. Hot-wire and pressure probes are too large to fit inside such spaces without causing significant flow disturbances and are not capable of responding to the high turbulence levels and flow reversals.

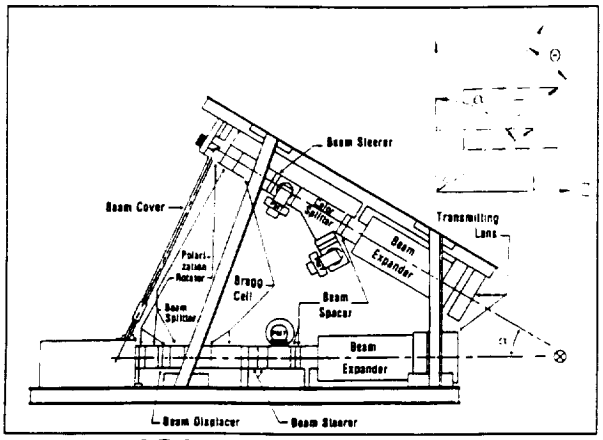

Figure 1 3-D Laser Doppler Anemometer System

EXPERIMENTAL APPARATUS

The Turbomachinery Laboratory at Texas A&M University designed a test facility for the measurement of the complex 3-D flow field inside journal bearings, annular seals, and labyrinth seals. The test facility includes a test flow loop, the test apparatus, and the laser Doppler anemometer system, all of which were specifically designed for this task. Figure 1 is a diagram of the 3-D laser Doppler anemometer system. An Argon-Ion laser was fitted with an air spaced etalon and allowed to lase at multiple wavelengths. A prism based color separator system was used to extract the 476, 488, and 514.5 nm lines from the composite beam. The 488 and 514.5 nm beams are passed through the lower optical train which is a standard 2-D LDA transmitting system which includes Bragg cells and an 8.5X beam expander. The 476 nm beam is transmitted through the upper optical train (also with a Bragg cell and 8.5X beam expander) which is inclined 30° above the lower train. The transmitting lenses are 450 mm focal length 152 mm diameter lenses. Each individual probe volume has dimensions of 0.032 mm X 0.032 mm X 0.26 mm (0.001" X 0.001" X 0.007") which compared to the clearance of the seal, 1.27 mm, would result in unacceptable spatial resolution. Therefore, an off-axis backscatter light collection scheme was implemented to reduce the effective size of the measurement volume. The top optical train receives the light reflected from the 488 and 514.5 nm beams transmitted from the lower train and the lower train receives the light reflected from the 476 nm beam. Each photodetector is equipped with a pinhole which acts as a spatial filter effectively producing a field of vision approximately 0.10 mm (0.004") in diameter. This results in an effective measurement volume of 0.032 X 0.032 X 0.10 mm (0.001" X 0.001" X 0.004").

A further benefit of this design is the reduction in the flare seen by the photomultiplier tubes. With a normal on-axis backscatter system the photomultiplier tube can become saturated by the flare (reflected light) generated by the laser beams hitting the wall several millimeters before the probe volume intersects the wall. The current arrangement minimizes this effect. Other techniques were also employed to enable near wall measurements which will be discussed later.

Figure 2 is a schematic of the test apparatus. A 50.8 mm (2 inch) overhung shaft is supported by two tapered roller bearings and powered by a 37 Kw (50 Hp) variable frequency drive. The outer housing is constructed of stainless steel with a small optical access port. The working fluid (water at the present time) enters from the right into a small plenum. A thick (12.7 mm) perforated plate (3.2 mm diameter holes) is used to eliminate swirl and distribute the water uniformly across the test section. Downstream of the plate, an axisymmetric inner plug

[1]Assistant Professor of Mechanical Engineering, University of Arkansas
[2]Design Engineer, Byron Jackson Pump Division of BW/IP

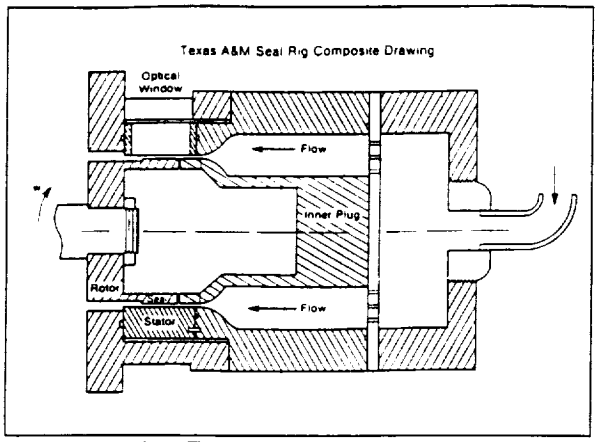

Figure 2 Seal Test Facility Schematic.

can be cantilever mounted from the perforated plate. The purpose of the plug and the contoured outer walls is to smoothly accelerate the fluid into the seal. An additional axisymmetric ring possessing small vanes can be mounted on the downstream end of the plug (just upstream of the rotor) to provide a know amount of preswirl to the fluid.

Water is supplied to the test apparatus by a 56 Kw (75 Hp) centrifugal pump via a turbine meter and throttling valve which are used to establish and maintain the flow rate. The water exiting the test apparatus is returned to a 15 m^3 (4,000 gallon) reservoir. The LDA system requires seed particles in the water. Expancel 461 was used (about a tea cup full) which has a specific gravity of 1.29 and a mean diameter of 6 $\mu m \pm 0.2\ \mu m$. This particle has a frequency response of 44 Khz in water which was deemed sufficient for the present study.

The particular annular seal being discussed in this paper is constructed of acrylic and has a rotor (journal) diameter of 0.163 m, a length of 37.3 mm, and a nominal clearance of 1.27 mm. In the current arrangement, the centerline of the shaft upon which the rotor is mounted is offset from the centerline of the rotor by 0.63 mm resulting in an eccentricity ratio of 50% and a rotor which is whirling at the same speed as the shaft.

An optical window was installed such that the entire length of the seal can be measured. The optical window is constructed of quartz and has a trapezoidal cross section (3.55 mm wide at the bottom {bush} expanding to 18.8 mm wide at top {outside}) and is 62.23 mm long. The top and bottom of the window are flat and parallel to each other to eliminate optical distortion and any focusing effect of the window. This is essential for the six beam LDA system being used since any lens effect limits the ability to traverse the probe volume about the flow field without continual realignment. The present design results in acceptable beam coincidence being maintained over a penetration depth of about 4 times the clearance (in water). The flat bottom of the window causes an out of roundness of the bush which is 0.027% of the rotor radius or 1.5% of the clearance.

The rotor was manufactured of clear acrylic and polished to obtain a smooth surface. The purpose of using acrylic is to reduce the amount of light reflected by the laser beams. This is very important in the present study since the laser beams must enter the test section along radial lines which produce significant amounts of flare (diffuse reflection) and specular reflection. In order to further minimize the light reflection an optical coating was applied to both the rotor and window. The quartz window's reflectance was decreased from 9.3% to 1.3% while the rotor's reflectance was decreased from 3.7% to 2% for 514.5 nm wavelength light. The rotor was coated using a special low temperature vacuum deposition technique.

Further considerations necessary to perform measurements inside the small gap (1.27 mm) included the orientation of the laser beams entering the test section. The natural tendency is to align the two optical trains symmetrically about the normal of the optical window. This generated a problem with specular light reflection from the window and rotor in that low power reflected beams were projected into the receiving optics and bounced around inside the optical train. This was unacceptable since the beam could hit the photomultiplier tube. Therefore, the LDA system was yawed with respect to the axial direction of the seal 9.8° so that reflected beams missed the receiving optics lenses. The yaw created a new problem in that the optical cone of light gathered by the receiving optics was distorted resulting in a blurred focal point. The greater the angle of yaw, the worse the distortion.

The alignment of the transmitting and receiving optics had to be done in situ due to the bending of the light as it traveled from the air into quartz and into water. The transmitting optics were aligned by using a 15 μm diameter high power pinhole mounted 0.63 mm (0.025") from the quartz window in the water. The high power pinhole was required so that heating by the laser beam did not cause distortion. Alignment was accomplished by blocking five of the beams and adjusting the remaining beam until it was centered in the pinhole. The beam was considered centered when a) maximum power was passing through the pinhole and b) the diffraction pattern generated by the beam passing through the pinhole was symmetric. Each beam was thus aligned through the pinhole assuring coincidence of the six beams at the probe volume.

The photomultiplier tubes were more difficult to align because the off-axis backscatter system results in a blurred side view of the probe volume. Additionally, the photodetector can be aimed at any location along the length of an individual probe volume (of which only 39% was located in the composite probe volume) and still receive valid Doppler bursts. In order to obtain coincident data, all three photodetector signals were displayed on a four channel oscilloscope. By triggering off the various photodetector signals, one can visually observe time lags between the Doppler bursts of the individual photodectectors. When all three photodetectors are focused on the same spatial location the time lags should be zero. This is evidenced by the presence of all three bursts occurring at the same time or at least within the 10 μs coincidence window used for these measurements.

The selection of the 10 μs coincidence window was determined by experimentally observing the correlation coefficients $\left[\frac{\overline{u_i' u_j'}}{\sqrt{\overline{u_i' u_i'}}\sqrt{\overline{u_j' u_j'}}}\right]$ between the various velocity components measured directly by the LDA for various coincidence window settings. Morrison, et al. [1991a] showed that in isotropic turbulence the correlation coefficient should equal the cosine of the angle between the velocity components. Since our system is measuring non-orthogonal velocity components, the technique can be applied to our data. This criterion has been used in our laboratory for many years and has been invaluable in validating the operating parameters used on the LDA. It was found that coincidence window settings larger than 10 μs resulted in a decreased correlation coefficient indicating poor coincidence. If coincidence is poor, the transformation of the velocity measurements from the non-orthogonal to an orthogonal coordinate system will yield an incorrect "on-axis" (Z direction in Figure 1) velocity component and components of the Reynolds stress tensor will be incorrect.

The present set of measurements involves a whirling annular seal. This requires a rotary encoding system which tags each data point with the angle of the rotor. Previous work (Morrison, et al. [1991b]) in non-whirling seals required 2,000

velocity vector realizations at each spatial location to obtain repeatable mean velocity and Reynolds stress tensor values. With the addition of the azimuthal dependence in the data, 90,000 velocity vector realizations were recorded at each axial-radial location in the present study and the results phase averaged to obtain the mean velocity and Reynolds stress tensor at 18 shaft phase angles. The number of velocity realizations at each phase angle varied from 1000 to 9000. The rotary encoding system was directly interfaced to the three counter systems used to validate the Doppler bursts. The McLaughlin-Tiederman [1973] velocity bias correction scheme was used on all of the data. This technique is easily applied to the 3-D data since the magnitude of each instantaneous velocity realization is obtained by the 3-D LDA system.

RESULTS

Mean Velocity

The mean axial, radial, and azimuthal velocities are shown in Figures 3 and 4. The rotor is whirling (precessing) in a clockwise direction. Upstream and at the inlet to the seal (Figures 3 and 4) the flow vectors on the pressure side are pointing inward. Upstream of the seal at Z/L=-0.02 (Figure 4), the mean axial velocity profile reaches a peak of greater than $0.9U_{ave}$ (6.6 m/s, where U_{ave}=7.4 m/s) between 60° and 135°. The radial velocities are generally pointed inward toward the seal because the flow has just been diverted inward by the curve in the plenum wall. The greatest inward mean radial velocities are located in the same region as the high U's. The inlet W does not exceed $0.08W_{sh}$ ($0.33U_{ave}$, 2.4 m/s) over most of the clearance.

At the seal inlet (Figure 3) the axial flow component begins to accelerate into the seal. The peak axial velocity is $1.5U_{ave}$ (11 m/s) across a band from 30° to 60° and stays above $0.5U_{ave}$ (3.7 m/s) across the entire circumference of the seal. The V profiles continue the strong inward trend. The maximum inward velocity reaches $-0.8U_{ave}$ (-6 m/s) from 45° to 190°. It appears that the inward momentum imparted to the flow by the curved stator wall is still affecting the fluid, but at the same time, the inlet shape of the seal is directing flow to the cavity under the seal. The tangential velocities begin to increase, with the $0.08W_{sh}$ (2.4 m/s) contour extending almost to the stator from 280° to 60°, and moving outward through the suction portion of the clearance.

Just downstream of the inlet at Z/L=0.04 (Figure 4) the axial velocities are much greater, with a maximum of $2.2U_{ave}$ (16.3 m/s) occurring at 95°. This peak is very close to the stator, and there are very high $\partial U/\partial r$ gradients on either side of the peak. A shear layer exists from 90° to 180°. A mild recirculation zone exists between the rotor and the shear layer with a maximum backflow velocity of $-0.1U_{ave}$ (-0.7 m/s). This recirculation zone occupies less than 15% of the clearance and is not visible on the figures. Reattachment of the axial velocity occurs at 180° where the axial velocities are significantly smaller than on the other side of the clearance. The axial recirculation produces a small vena contracta. The V profile changes significantly at this point, as the direction of the velocities is redirected back out toward the stator. A maximum of $0.18U_{ave}$ (1.3 m/s) at 45° is surrounded by mild $\partial V/\partial r$ gradients on either side. The radial velocities are pointed outward near the rotor and inward near the stator on the wide clearance side of the rotor, indicating the presence of a vena contracta around 135°. Because the axial momentum in this area is so small, the tangential velocities are able to develop quickly, especially in the recirculation zone where $W=0.24W_{sh}$ (6.9 m/s, $0.9U_{ave}$) in the middle of the clearance from 60° to 280°.

From Z/L=0.04 to Z/L=0.07 (Figure 4) the axial velocities decrease, only reaching a maximum of $1.9U_{ave}$ (14 m/s) at θ=120°. The high velocity area is still along the stator, and the steep $\partial U/\partial r$ gradients near the rotor surface are relaxing. The recirculation zone has disappeared along the rotor, but the velocities are still very low there. The disappearance of the shear layer implies that the axial streamlines have reattached to the rotor. The radial velocities are directed back out toward the stator after turning at the reattachment point. The tangential velocity development diminished with the reattachment of the axial velocity streamlines.

Moving to Z/L=0.14 (Figure 4), the U profile is more evenly distributed throughout more of the seal, as the peak axial momentum region reaches wider clearances, which is decelerating the flow. The peak axial velocity is $1.5U_{ave}$ (11 m/s) and it is located at 90°. The rest of the profile remains attached to the rotor and stator with very mild $\partial U/\partial r$ gradients. The axial velocity on the suction side of the rotor is steadily increasing, with the minimum continuous contour at $0.7U_{ave}$, where just upstream it is $0.6U_{ave}$. The radial velocities continue to decrease in magnitude and now are fairly insignificant. The decrease in axial momentum is acting favorably for the tangential velocities, which are now increasing over the entire seal. The $0.08W_{sh}$ (2.4 m/s) level is now extending much further into the maximum clearance region, and it is distributed more uniformly.

From Z/L=0.14 to Z/L=0.50 (Figure 3) the trends discussed above continue; the axial velocity continues to spread more uniformly across the entire seal, the radial velocities remain small, and the tangential velocities increase with the decrease in axial momentum. At the midplane the axial velocity profile is almost uniform, with regions in the maximum clearance area having velocities which are a little higher. As the location of the maximum axial velocity rotates around the seal, the negative radial velocity zone also moves. By the midplane it is relocated to the minimum clearance region. The tangential velocity develops to $0.08W_{sh}$ all the way out to the stator, and it is increasing in the pressure section of the clearance, reaching $0.16W_{sh}$ (4.8 m/s) by the midplane.

Farther down the seal at Z/L=0.77 the location of the maximum axial velocity is convected around the seal by the increasing tangential velocity component. The peak axial velocity is at 240° and has increased to $1.4U_{ave}$ (10.4 m/s) as the tangential component is forcing the fluid into a smaller region. The radial velocity is similar to that upstream, with positive values pointing out from the rotor and negative in from the stator. The tangential profile develops significantly, with the $0.24W_{sh}$ (6.9 m/s) zone extending almost entirely across the pressure zone around 60°. This significant increase in the tangential momentum is the mechanism driving the axial velocity peak around to the other side of the clearance.

The axial velocities on the suction side of the clearance continue to increase as the flow progresses downstream while the tangential velocities increase on the pressure side. This continues to the exit plane where the peak axial velocity reaches $1.7U_{ave}$ (12.6 m/s) at 265°. At the exit plane nearly the whole pressure side of the clearance is dominated by tangential velocities of at least $0.24W_{sh}$ (0.93U) and on the suction side they are $0.16W_{sh}$ (4.6 m/s). The radial profile remains virtually unchanged through the rest of the seal, not exceeding $0.08U_{ave}$ (0.6 m/s). The radial velocities are pointed inward along the stator.

Turbulence Levels

Upstream of the inlet, in the plenum at Z/L=-0.02 (Figure 4), the axial normal Reynolds stress term is extremely subdued, which is reflected in the mild gradients in the mean velocity terms. The $\overline{u'u'}$ term barely reaches more than $0.05U_{ave}^2$ (2.7 m^2/s^2). At the inlet (Figure 3) the front edge of the rotor causes changes. The $\overline{u'u'}$ term builds (exceeding $0.33U_{ave}^2$, 18 m^2/s^2) along the rotor surface on the bottom side where the recirculation zone is located a bit farther downstream.

(Note: the recirculation is evident in the numerical data but does not appear in the contour plots.) This stress decelerates the axial velocity at the surface of the rotor. By Z/L=0.07 (Figure 4), the $\overline{u'u'}$ value decreases with the large gradients also showing a marked reduction. The peak of the $\overline{u'u'}$ stress is transported to 110° by the tangential momentum, and the peak has diminished. Dissipation dominates the flow at this point, where upstream turbulence production is the major mechanism, and works to distribute the turbulence term fairly evenly by midplane, Z/L=0.50. The profile remains reasonably uniform on the suction side, but by the exit plane, Z/L=1.00, there are again high values of $\overline{u'u'}$. Although the gradients are steep, it seems likely that the phenomenon is real because of the circumference over which it is distributed. The turbulence producing source at this plane is the step at the end of the seal.

CONCLUSIONS

A 3-D LDA has been used to successfully measure the velocity field in a whirling annular seal. To accomplish this a number of techniques had to be used including

- use of a transparent surface on the far side of the probe volume,
- optical coating of all transparent surfaces,
- special beam alignment techniques,
- off angle (i.e. not 180°) backscatter light collection,
- use of 8.5X beam expanders to provide a very small measurement volume,
- use of the smallest coincidence window available at the time,
- and use of a rotary encoder interfaced with the signal processors to permit phase information to be collected.

With the application of these techniques it was possible to measure a very complex internal flow field and to find some interesting results. At the inlet the highest axial velocities occurred in the region with the smallest clearance, forced by the upstream conditions. The axial momentum rotates the high axial velocity around the seal until it is on the opposite side by the exit, i.e. a map of maximum axial velocity traces a helix longitudinally through the seal. The radial velocities are driven by the greater axial and azimuthal velocities. As the flow separates across the inlet to the seal, the axial turbulence intensity jumps dramatically and causes the flow to decelerate. The region of maximum axial velocity fluctuations maps in a manner similar to the mean values. The exit induces another increase in the axial Reynolds stress.

The picture which develops is significantly different than is seen in an eccentric seal without the rotor whirling, Johnson [1989]. Although often experimental measurements confirm expectations developed by intuition, results such as these should provide the impetus for continued experimental measurements to ensure that erroneous assumptions about the flow fields are not adopted.

DATA AVAILABILITY

The data used for the preparation of this paper along with the entire Reynolds stress tensor are available in tabular form and on MS-DOS floppy disks.

ACKNOWLEDGEMENTS

This research was sponsored by the NASA Lewis Research Center under the supervision of Mr. Robert Hendricks and by the Texas A&M University Turbomachinery Research Consortium.

NOMENCLATURE

A	Leakage area, m^2
c	Mean clearance between the stator and rotor, m
d	Rotor diameter, m
e	Eccentricity, m
L	Length of the seal, m
Q	Leakage flow rate, m^3/s
r	Radial distance from stator centerline, m
Re	Reynolds number = $2Uc/\nu$
Ta	Taylor number = $\frac{cW_{sh}}{\nu}\sqrt{\frac{2c}{d}}$
U	Axial mean velocity, m/s
U_{ave}	Bulk mean velocity=Q/A, m/s
V	Radial mean velocity, m/s
W	Tangential mean velocity, m/s
$\overline{u'u'}$	Time averaged Reynolds stress, m^2/s^2
W_{sh}	Rotor surface speed, m/s
Z	Distance downstream of the seal inlet, m
ϵ	Eccentricity ratio, e/c
θ	Azimuthal angle measured in the direction of rotation from the minimum clearance
μ	Fluid absolute viscosity, (N s)/m^2
ν	Kinematic viscosity, m^2/s
ρ	Fluid density, kg/m^3
ω	Whirl ratio, ω_p/ω_r
ω_p	Rotor precession speed, rpm
ω_r	Rotor speed, rpm

REFERENCES

Johnson, M.C., 1989, "Development of a 3-D Laser Doppler Anemometry System: With Measurements in Annular and Labyrinth Seals," Ph.D. Dissertation, Texas A&M University, College Station, Texas, 77843.

McLaughlin, D.K. and Tiederman, W.G., 1973, "Bias Correction for Individual Realization of Laser Anemometer Measurements in Turbulent Flows," *The Physics of Fluids*, Vol. 16, pp. 2082-2088.

Morrison, G.L., Johnson, M.C., Swan, D.L., DeOtte, R.E., 1991a, "Advantages of Orthogonal and Non-Orthogonal 3-D Anemometer Systems," *Flow Measurement and Instrumentation*, Vol. 2, pp. 89-97

Morrison, G.L., Johnson, M.C., and Tatterson, G.B., 1991b, "Three-Dimensional Laser Anemometer Measurements in an Annular Seal," *ASME Journal of Tribology*, Vol. 113, pp. 421-427.

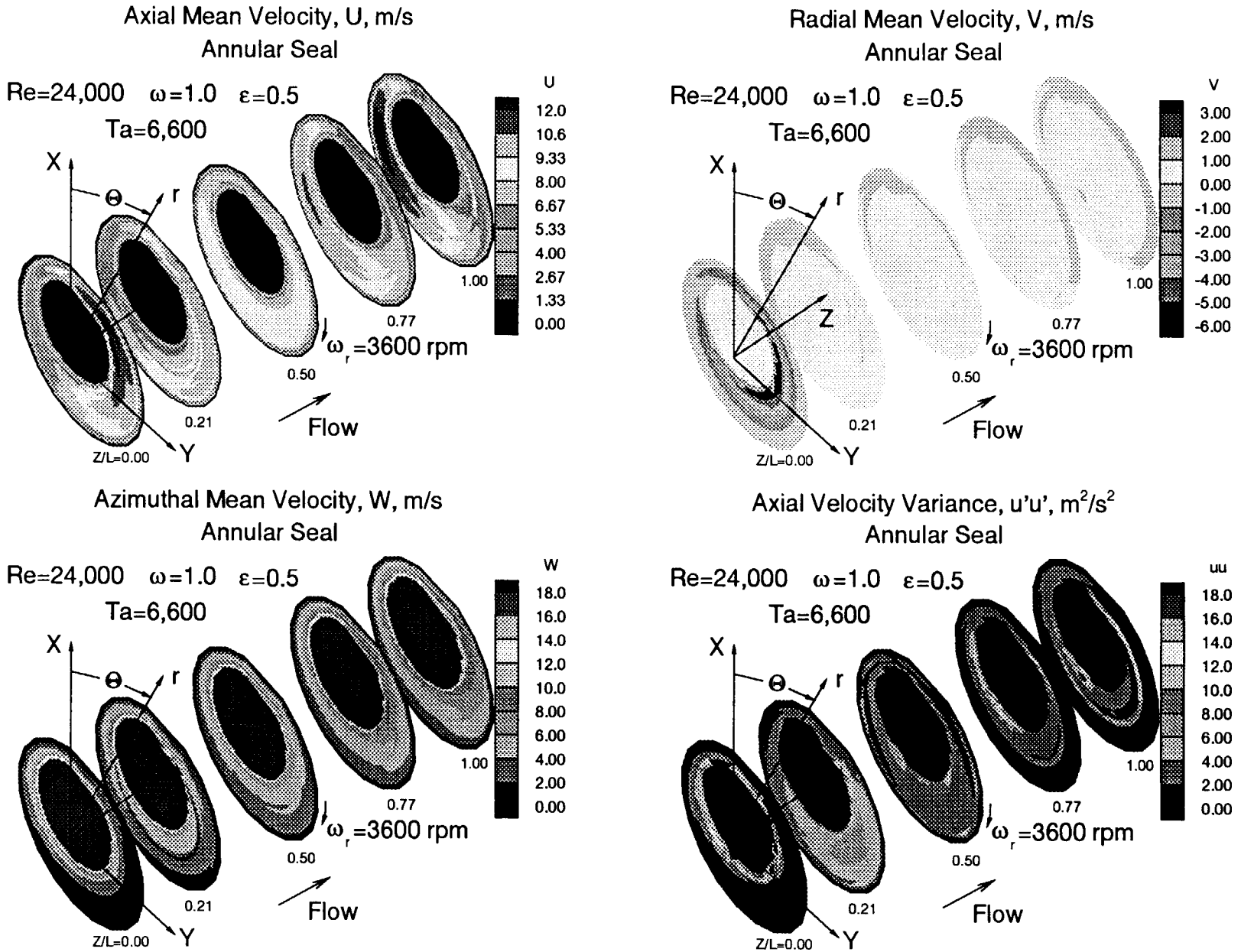

Figure 3. Mean velocity and axial velocity variance, Re=24,000, $0.00 \leq Z/L \leq 1.00$.

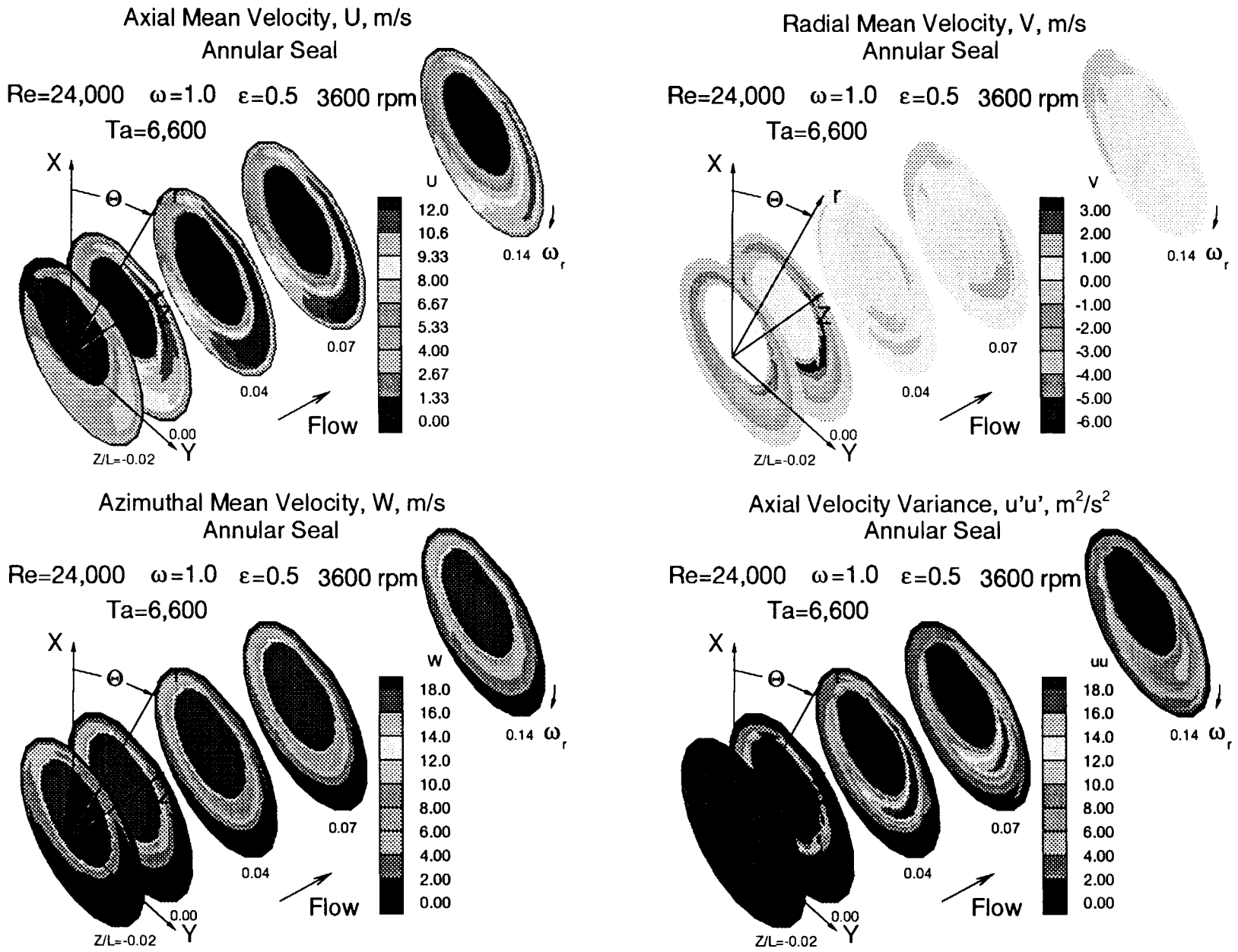

Figure 4. Mean velocity and axial velocity variance, Re=24,000, $-0.02 \leq Z/L \leq 0.14$.